Versatile Interactions of the Antimicrobial Peptide Novispirin with Detergents and Lipids†

Reinhard Wimmer,‡ Kell K. Andersen,‡ Brian Vad,‡ Mads Davidsen,‡ Søren Mølgaard,‡ Lise W. Nesgaard,‡ Hans H. Kristensen,§ and Daniel E. Otzen*,‡

Department of Life Sciences, Aalborg University, Sohngaardsholmsvej 49, DK-9000 Aalborg, Denmark, and Novozymes A/S, DK-2880 Bagsvaerd, Denmark

Received September 15, 2005; Revised Manuscript Received November 11, 2005

ABSTRACT: Novispirin G-10 is an 18-residue designed cationic peptide derived from the N-terminal part of an antimicrobial peptide from sheep. This derivative is more specific for bacteria than the parent peptide. We have analyzed Novispirin's interactions with various amphipathic molecules and find that a remarkably wide variety of conditions induce α-helical structure. Optimal structure induction by lipids occurs when the vesicles contain 40−80% anionic lipid, while pure anionic lipid vesicles induce aggregation. SDS also forms aggregates with Novispirin at submicellar concentrations but induces α-helical structures above the cmc. Both types of aggregates contain significant amounts of *β*-sheet structure, highlighting the peptide's structural versatility. The cationic detergent LTAC has a relatively strong affinity for the cationic peptide despite the peptide's net positive charge of +7 at physiological pH and total lack of negatively charged side chains. Zwitterionic and nonionic detergents induce α-helical structures at several hundred millimolar detergent. We have solved the peptide structure in SDS and LTAB by NMR and find subtle differences compared to the structure in TFE, which we ascribe to the interaction with an amphiphilic environment. Novispirin is largely buried in the SDS−micelle, whereas it does not enter the LTAC−micelle but merely forms a dynamic equilibrium between surface-bound and nonbound Novispirin. Thus, electrostatic repulsion can be overruled by relatively high-detergent concentrations or by deprotonating a single critical side chain, despite the fact that Novispirin's ability to bind to amphiphiles and form α-helical structure is sensitive to the electrostatics of the amphiphilic environment. This emphasizes the versatility of cationic antimicrobial peptides' interactions with amphiphiles.

Widespread use of conventional antibiotics has resulted in an increasing number of multiresistant microorganisms that pose a problem when dealing with infections and sepsis. In the search for alternatives to traditional antibiotics, antimicrobial peptides (AMPs)[1] have emerged as a possible solution (*1*). These peptides are a part of the innate immune system of almost all kingdoms, ranging from bacteria to animals, indicating that AMPs are an important part of evolution (*2*). The AMPs offer a quick immune response to a broad range of microbes. This is important because the activation of the pathogenic immune response is slow compared to microbial proliferation (*3*). AMPs show enormous sequence diversity but have been classified into four groups. These include linear peptides with or without a hydrophobic C-terminus which form α-helices upon binding to membranes, peptides containing a rigid antiparallel *β*-sheet held together by disulfide bonds, and linear peptides rich in one or two amino acids such as Trp, Pro, or Arg (*2*).

Whatever their structure, AMPs tend to be both amphipathic and cationic. Amphipathicity increases their affinity for biological membranes, while the positive charge increases their specificity toward negatively charged bacterial membranes, instead of the more neutral membrane surrounding eukaryotic cells. Interestingly, this preference for negatively charged membranes is also seen for aggregating proteins such as α-synuclein (*4*), and the ability of such proteins to bind and permeabilize membranes has been suggested to be a central phenomenon in the development of Parkinson's Disease and other dementias (*5*). Unfortunately, several AMPs have shown cytotoxic and hemolytic effect. Current models of AMP action suggest that the peptides bind and disrupt the cell membrane, either by forming holes through

† Daniel E. Otzen is supported by the Villum Kann Rasmussen Foundation and the Danish Research Foundation. Financial support from the Obel Foundation to both R.W. and D.E.O. is gratefully acknowledged.

* To whom correspondence should be addressed. E-mail: dao@bio.aau.dk. Tel: + 45 96 35 85 25. Fax: + 45 98 14 18 08.

‡ Aalborg University.

§ Novozymes A/S.

[1] Abbrevations: 2QF-COSY, double quantum filtered correlation spectroscopy; AMP, antimicrobial peptide; ATR, attenuated total reflection; CD, circular dichroism; CMC, critical micelle concentration; DM, dodecyl maltoside; DOPC, 1,2-dioleoyl-*sn*-glycero-3-phosphocholine; DOPE, 1,2-dioleoyl-*sn*-glycero-3-phosphoethanolamine; DOPG, 1,2-dioleoyl-*sn*-glycero-3-[phosphor-rac-(1-glycerol)]; DPS, 3-(dodecyldimethylammonio)propanesulfonate; EDTA, ethylenediamine tetraacetate; HPLC, high-performance liquid chromatography; IPTG, isopropyl-*β*-D-thiogalactopyranoside; KSI, kesteroid isomerase; LTAB, lauryl-trimethylammonium bromide; LTAC, lauryl-trimethylammonium chloride; MALDI-TOF, matrix-assisted laser desorption ionisation-time-of-flight; NOESY, nuclear Overhauser effect spectroscopy; NPN, 1-*N*-phenylnaphthylamine; PAGE, polyacryl gel electrophoresis; PBS, phosphate buffer saline; PFG, pulsed field gradient; SDS, sodium dodecyl sulfate; TFA, trifluoro acetic acid; TFE, 2,2,2-triflour ethanol; TOCSY, total correlation spectroscopy.

10.1021/bi051876r CCC: $33.50
Published on Web 12/15/2005

the membrane (the barrel-stave model) or by disturbing the lipid arrangement in the outer leaflet (the carpet model), leading to growth inhibition or lysis (*6*−*8*). Until now, only very little resistance has been observed against AMPs (*9*), and the few reported cases involve a reduction in the amount of acidic lipids or the production of specific digestive proteases (*2*).

Besides their direct antimicrobial effect, the AMPs have also proven to have other important roles such as stimulation of adaptive immunity by recruiting memory T-cells and immature dendrite cells (*10*), binding to and inactivating toxic bacterial lipopolysaccharides (*11*), and binding to cellular receptors and activating signaling pathways (*12*).

A number of biophysical features have emerged that influence the interaction between AMPs and membranes. First, electrostatic attraction is very important for initial binding to the membrane surface. Work with synthetic liposomes suggest that negative lipids must be included to achieve high affinity, while screening charge by the presence of salt can reduce or destroy AMP antimicrobial activity (*13*−*15*). Second, interactions with the hydrophobic parts of the membrane are important for the energetics of pore formation. The specific composition of the membrane can be expected to affect the energetics of pore formation through parameters such as bilayer thickness and degree of order, curvature strain, and adsorption energy (*8*, *16*, *17*). Thus, incorporation of PE lipids, which leads to reduced strain in the surface-bound peptide−lipid complex, increases the [peptide]/[lipid] ratio needed for pore formation (*18*), while DOPC encourages membrane insertion to a larger extent than the thinner DLPC (*19*). In addition, physiological features such as membrane proteins, periplasmic components, membrane potential and pH gradients, efflux pumps, and so forth (*20*) can also influence the process of membrane insertion.

Detergents mimic the amphiphilic nature of lipids, but do not provide the bilayer environment needed for pore formation by AMPs. Thus, the interaction between detergents and α-helical AMPs allows us to focus on the first stage of the pore-forming process, namely, binding and formation of α-helical structure. Because of the cationic nature of the AMPs, the anionic detergent SDS is the most popular detergent for such studies (*21*), although a zwitterionic detergent like dodecylphosphocholine can also induce α-helical structure at similar detergent concentrations (*22*). In contrast, nonionic detergents are generally not so effective at inducing structure (*23*), and cationic detergents have, to our knowledge, not been reported to interact significantly with cationic microbial peptides (*24*).

Micellar SDS has, for a long time, been known to stabilize α-helical conformations, even in peptides derived from *β*-sheet structures (*25*). For cationic sequences, this has been shown to be mediated by stable salt bridges between positively charged amino acids and the sulfate group of SDS (*26*), while more hydrophobic sequences probably penetrate into the hydrophobic micellar core (*27*). Because of the specific interactions involved, detergent chain length and headgroup structure can influence the degree of α-helicity of the bound peptide. For example, the helical part of a 15-residue membrane targeting peptide was one residue shorter in sodium nonanesulfonate and 3 residues shorter in sodium hexanesulfonate than in SDS (*28*); SDS was also shown to lead to a structure closest to that observed in the presence of the short chain lipid didecanoyl phosphocholine. The small size of the peptide relative to the detergent means that the micelle size is hardly influenced by the peptide (*28*).

Novispirin is a synthetic peptide (sequence KNLRR IIRKI IHIIK KYG), developed in several steps from the N-terminal part of the 29 residue α-helical AMP SMAP-29 found in sheep. SMAP has shown unusually potent antimicrobial activity (*29*), but its haemolytic and cytotoxic properties have excluded use in humans. Therefore, residues have been introduced which enhance helix stability and create a more pronounced gradient of hydrophobicity along the backbone. This resulted in enhanced bacterial activity and salt tolerance, and the additional Ile → Gly mutation in position 10 decreased haemolytic activity sufficiently to make it a suitable candidate for human use (*30*). The structure of Novispirin in 40% TFE reveals an α-helix from residue 3 to 11, a hinge formed by His12 and Ile 13, and a 3_{10} helix from residue 14 to 16 (*30*). Alcohols such as TFE are known to stimulate α-helix formation (*31*, *32*), probably due to the decrease in solvent polarity which strengthens hydrogen bonding, as well as direct binding to the peptide or protein.

Here, we describe structural studies on the AMP Novispirin G-10 in the presence of different lipids and detergents. The objective was to obtain a better understanding of the relative contributions of electrostatic and hydrophobic effects when Novispirin folds in an amphiphilic environment. Not surprisingly, zwitterionic lipids alone are not able to induce an α-helical structure in Novispirin at experimentally accessible concentrations, unless at least 20% anionic lipid is included. Zwitterionic and nonionic detergents induce an α-helical structure, albeit several orders of magnitude more weakly than SDS. Interestingly, the cationic detergent LTAC is able to induce α-helical structure in Novispirin at detergent concentrations comparable to SDS, although there were subtle changes in the far-UV CD spectrum. We therefore carried out a comparative analysis of the structure and micelle interactions of Novispirin in SDS and LTAB by NMR spectroscopy. To our knowledge, this is the first atomic-level study to address interactions between cationic detergents and antimicrobial peptides.

The peptide formed a helical secondary structure in both SDS and LTAB, although the [detergent]/[peptide] ratio needed to induce secondary structure formation was much higher in LTAB than in SDS. Several NMR techniques were applied to gather information about the relative positioning of the peptide within/on the detergent micelle: H^N-exchange, NOE cross-peaks between the peptide and the lipid, and the addition of paramagnetic ions. These techniques revealed that Novispirin is, to a good part, buried in the SDS−micelle, whereas it does not enter the LTAB−micelle but forms a dynamic equilibrium between surface-bound and nonbound Novispirin. Such a dynamic equilibrium can explain how detergents can override electrostatic repulsion at sufficiently high-detergent concentrations.

MATERIALS AND METHODS

Materials. All lipids, namely, DOPC, DOPE, and DOPG, were from Avanti Polar Lipids (Alabaster, AL). Sodium-dodecyl-d_{25}-sulfate, LTAC, DPS, NPN, and Lipopolysaccharide EH100 from *Escherichia coli* were from Sigma. DM was from Calbiochem and TFE from Aldrich. All chemicals

were of the highest grade available. LTAB-d_{25} (deuterated only on the dodecyl chain but not on the methyl groups) was obtained from QMX Laboratories (U.K.). Note that LTAB-d_{25} was only used for NMR experiments, where deuterated detergent was necessary due to the availability of the deuterated form; for other experiments, LTAC was used due to its lower absorption in the far-UV area.

Cloning, Expression, and Purification of Novispirin G-10. For economy of scale, Novispirin G-10 (KNLRRIIRKGIHIIKKYG) was produced recombinantly in *E. coli* as inclusion bodies. This was achieved through gene-fusion with a fragment of KSI using the commercially available plasmid pET31b+ (www.novagen.com). To facilitate downstream processing and recovery of Novispirin G-10, the Novispirin G-10 gene was preceded by an aspartate−proline (DP) dipeptide, followed by an aspartate−glutamate dipeptide (DE). Thus, the gene-fusion construct encodes the following: KSI−D−P−D−E−NovispirinG-10. The DP dipeptide is prone to mild acid hydrolysis at elevated temperatures (*33*, *34*), and the glutamic acid residue located immediately upstream of the Novispirin G-10 is substrate of a glutamyl endopeptidase I.

The expression plasmid was constructed using the following oligonucleotides encoding Novispirin G-10: (5′-ATT ATT CAG ATG CTG GAT CCG GAC GAA AAA AAC CTG CGT CGC ATT ATC CGC AAA GGC ATC CAT ATC ATT AAA AAA TAT GGC TAA TAA CTC GAG ATT ATT-3′ and 5′-AAT AAT CTC GAG TTA TTA GCC ATA TTT TTT AAT GAT ATG GAT GCC TTT GCG GAT AAT GCG ACG CAG GTT TTT TTC GTC CGG ATC CAG CAT CTG AAT AAT-3′). Enzymatic digestion of introduced flanking restriction endonuclease sites (AlwNI/AvaI) enabled the cloning of the synthetic gene as a fusion construct in pET31b+ (standard procedures as described by the manufacturer (New England Biolabs, Inc., MA)). All standard protocols have been described elsewhere (*35*).

Recombinant pET31b+ was transformed into *E. coli* Novablue as described by the manufacturer (Novagen). Plasmids were recovered by QIAprep Mini Columns (QIAGEN, Inc., CA) and sequenced by automated sequencing using plasmid-specific primers (5′-TGC TAG TTA TTG CTC AGC GG-3′ and 5′-ACC GTA GTT GCG CCC ATC G-3′). Recombinant plasmid was transformed in *E. coli* BLR-DE3 according to the manufacturer (Novagen). Bacteria were cultivated in LB media to $OD_{600} \sim 0.8$, and recombinant protein synthesis was initiated by 1 mM IPTG. Three hours after induction, bacteria were harvested, resuspended in $^1/_{10}$ volume buffer A (50 mM Tris-HCl, 1 mM EDTA, and 100 mM NaCl, pH 8), and lysed by pressure disruption (1500 mbar). The DPDE−Novispirin G-10 is located in inclusion bodies, which were isolated by centrifugation at 24 000*g* for 2 h. The resulting inclusion body pellet was washed twice in buffer B (50 mM Tris-HCl, 10 mM EDTA, 0.5% Triton X-100, and 100 mM NaCl, pH 8). All standard protocols have been described elsewhere (*35*).

The PDE−Novispirin G-10 was liberated from the inclusion bodies by hot acid hydrolysis, which cleaves specifically between Asp−Pro. This sequence was introduced between the KSI (ketosteroid isomerase) fusion partner and N-terminally to the synthetic gene encoding Novispirin G-10. For hot acid hydrolysis, inclusion bodies were resuspended in 100 mM sodium phosphate (pH 2.3) and incubated overnight at 85 °C. Resulting supernatant contained PDE−Novispirin G-10. The sample was neutralized by adding 100 mM sodium phosphate (pH 12.3). The peptide was matured with a glutamyl endopeptidase I from *Bacillus licheniformis* (*36*) produced by Novozymes A/S.

The matured octadecapeptide was purified by cation-exchange chromatography, as follows. The Novispirin G-10 and glutamyl endopeptidase mixture was adjusted to pH 6 and 7 mS/cm prior to application to a CM−sephadex column (Amersham Biosciences). Novispirin G-10 was eluted with a 0−1 M NaCl gradient in 50 mM malonic acid, pH 6, over 10 CV. The fractions were analyzed by MALDI-TOF mass spectrometric analysis (for Novispirin identification) and SDS−PAGE (for high MW impurity detection). The selected fractions were pooled and desalted on Sephadex-G10 column (Amersham Biosciences) equilibrated with PBS, pH 7.4 (50 mM phosphate buffer and 150 mM NaCl). Again the fractions were analyzed by MALDI-TOF mass spectrometric analysis and pooled. The Novispirin G-10 pool was analyzed for purity by SDS−PAGE and RP-HPLC (Jupiter, 5 μm, C18 300 Å, 150 mm × 2 mm, 50 min gradient from 8 to 80% acetonitrile in 0.1% triflouric acid, flow of 0.15 mL/min, $\lambda = 214$ nm). The identity of the peptide was determined by automated N-terminal sequencing using a Procise automatic sequencer (Applied Biosystems Division, Perkin-Elmer), and the concentration was determined by amino acid analysis performed on a Biochrom 20 Plus (Biochrom, Ltd.).

MALDI-TOF Mass Spectrometric Analysis. A 0.5 mL sample was spotted onto a stainless steel target plate. A volume of 0.5 μL of 10 mg/mL 4-hydroxy-α-cyano-cinnapinic acid (HCCA) in 50% acetonitrile and 0.1% TFA was subsequently mixed with the sample on the target plate. The sample spots were allowed to dry at room temperature before analysis (dried droplet method). MALDI analyses were performed on a Voyager DE Pro mass spectrometer with delayed extraction technology and a 337 nm N_2 laser producing 3 ns pulses with a repetition rate of 20 Hz (Applied Biosystems). The instrument was run in reflective mode with positive ionization. External calibration was applied using CalMix2 (Applied Biosystems).

Preparation of Vesicles. Synthetic lipid samples were mixed from stock solutions of lipids dissolved in methanol and dried overnight in a Heto VR-1 centrifuge vacuum drier. Lipids were then resuspended by vortexing in 20 mM sodium phosphate, pH 7.5, to a final concentration of 5 g/L (∼7 mM), exposed to at least seven cycles of freezing in liquid nitrogen, followed by thawing in a 55 °C water bath, before extrusion through a 100 nm pore filter (Nucleopore track etch membrane (Whatman)) 12 times using a 10 mL thermobarrel extruder (Northern Lipids, Vancouver, Canada). Vesicle sizes were confirmed by dynamic light scattering (DynaPro 99, ProteinSolutions). All extruded vesicles were used within 2 days of production. *E. coli* total lipid extract was not extruded due to its high content of phosphoethanolamine lipids but was subjected to 60 min of sonication in a sonication bath after the freeze−thaw step. This yielded a clear solution of vesicles with a hydrodynamic radius of around 75 nm as measured by dynamic light scattering.

CD Spectroscopy. All experiments were carried out in 20 mM sodium phosphate, pH 7.5, at 25 °C unless otherwise stated. Experiments at pH 11 were carried out using 20 mM

Gly as buffer. Equilibrium circular dichroism studies were performed on a Jasco J-810 spectropolarimeter (Jasco Spectroscopic Co., Hachioji City, Japan) with a Jasco PTC-348W1 temperature control unit. At least four scans were averaged to yield the final spectrum. Unless otherwise stated, the peptide concentration was 40 μM, and a 1 mm quartz cuvette was used.

FTIR Spectroscopy. All experiments were carried out in 20 mM Tris, pH 7.5, at 25 °C and at a peptide concentration of 40 μM. Fourier transform infrared spectroscopy was carried out on a Bruker Tensor 27 infrared spectrometer (Bruker Optik GmbH, Ettlingen, Germany) with a Specac Golden Gate single-reflection ATR unit (Specac, Ltd., Orpington, U.K.). The peptide was precipitated in 0.75 mM SDS or 1 mM DOPG. Aggregates were isolated by centrifugation and resuspended in 0.75 mM SDS or 0.2 mM DOPG. Samples were prepared by drying on the ATR surface under a gentle stream of nitrogen. Spectra were recorded with 128 accumulations and analyzed using OPUS 5.5 software (Bruker Optik GmbH, Ettlingen, Germany). For the DOPG samples, a DOPG spectrum was collected and subtracted from the sample spectra to remove the C═O peak at 1740 cm^{-1}. Estimates of secondary structure were obtained by fitting of Gaussian curves by the Levenberg Maquardt method. The number of bands and the positions were determined from the second derivative spectrum and by Fourier self-deconvolution as described (*37*). Bands were grouped by secondary structure type, and the relative band area percentages were calculated.

For comparison with results from CD spectroscopy, transmission spectra were recorded in D_2O using 2 mg/mL Novospirin in 85 mM SDS and 20 mM Tris, pH 7.5.

Determination of Critical Micelle Concentration (Cmc). Cmc was determined by monitoring the conductivity as a function of detergent concentration in the appropriate buffers using a CDM210 conductivity meter (Radiometer, Denmark). The cmc was defined as the detergent concentration where the increase in conductivity with detergent concentration kinks to a lower slope.

Data Analysis. To obtain a quantitative measure of the affinity of Novispirin for different lipids and detergents, titration data (CD signals versus detergent or lipid concentration) were fitted to the following equations.

(1) Hyperbolic binding (only for LPS, DM, DPS, and LTAC):

$$S = S_{\text{start}} + \Delta S \frac{[\text{det}]}{[\text{det}] + K_{\text{d}}} \quad (1)$$

where ΔS is the signal change between the free and bound Novispirin and K_{d} is an apparent binding constant.

(2) Cooperative binding (sigmoid curve):

$$S = \frac{S_{\text{end}} + S_{\text{start}} 10^{-c(L-L_{50\%})}}{1 + 10^{-c(L-L_{50\%})}} \quad (2)$$

where S_{start} and S_{end} are the CD values at low- and high-lipid concentrations, respectively, concentration L, $L_{50\%}$ is the concentration at which the transition is halfway to completion, and c is the cooperativity constant. The lower c is, the more gradual the transition.

NMR Recording. All NMR spectra were recorded on a BRUKER DRX600 spectrometer operating at a field strength of 14.1 T, equipped with a TXI(H/C/N) probe with triple-axis gradients. Spectra were processed using XWinNMR 2.6 and 3.6.

Titration of Novispirin in LTAC. 1. Constant pH. A sample of novispirin was dissolved in 550 μL of a solution containing 80 mM NaCl, 3 mM NaN_3, 20 mM phosphate buffer, and 5% D_2O. The peptide concentration was 2.5 mM. The pH was adjusted to 5.7 by addition of 1 M H_3PO_4. Solid LTAC was added in small amounts directly into the NMR sample tube. The volume increase (20% at 1 M LTAC) was estimated by help of a graduated sample tube; LTAC concentrations were corrected for the increase in volume. No measures were taken to keep the peptide or salt concentrations unchanged. For each concentration of LTAC, a 1D NMR spectrum and a diffusion spectrum were measured. The 1D NMR spectrum was measured using excitation-sculpting water suppression (*38*) and selective excitation of the region from 6 to 9 ppm by an off-resonance Q5 pulse (*39*) of 3.14 ms duration. This ensured maximum sensitivity on the peptide H^N/aromatic signals by leaving detergent magnetization in the longitudinal state. Experimental details of the diffusion measurements are described below.

2. Constant [LTAC]. A sample of novispirin was dissolved in 550 μL of a solution containing 270 mM LTAC, 80 mM NaCl, 3 mM NaN_3, 20 mM phosphate buffer, and 5% D_2O. The peptide concentration was 2.5 mM. The pH was brought to 9 by addition of 1 M NaOH; thereafter, pH was brought to 4.6 in steps of approximately 0.5 pH units by addition of 1 M H_3PO_4. A 1D NMR spectrum was measured using excitation-sculpting water suppression (*38*) and selective excitation of the region from 6 to 9 ppm by an off-resonance Q5 pulse (*39*) of 3.14 ms duration at each pH value. The solution was diluted by approximately 7% in the course of the titration; no action was taken to compensate for this.

Structure Determination. 1. SDS. The NMR sample was prepared by dissolving novispirin in 350 μL of a 300 mM SDS-d_{25} (Sigma-Aldrich), 300 mM NaCl, 3 mM NaN_3, and 20 mM phosphate buffer solution containing 5% D_2O. The pH of the solution was brought to 4.6 by addition of 1 M H_3PO_4. A 2D NOESY spectrum with 70 ms mixing time was recorded with a WATERGATE water suppression (*40*). [^{1}H,^{1}H]-TOCSY spectra with 40 and 80 ms mixing time, respectively, were recorded using the clean-TOCSY sequence (*41*) with a 15 kHz spin-lock and a WATERGATE water suppression. In addition, a 2QF-COSY experiment was recorded. The assignment was obtained by following the sequential assignment procedure outlined in ref *42*. Spectral analysis was performed with XEASY (*43*) and its PC version NEASY. The temperature for the experiments with SDS was chosen to be 50 °C, since signal intensities at lower temperatures were dissatisfactory, probably due to fast transverse relaxation brought about by high correlation times of the large micellar particles.

2. LTAB. The NMR sample with LTAB was prepared by adding LTAB-d_{25} to a final concentration of 1 M to a solution of 3.1 mM Novispirin in 20 mM phosphate buffer containing 80 mM NaCl and 3 mM NaN_3. The pH was brought to 5.7 by addition of 1 M H_3PO_4. The necessary concentration of LTAB had been determined by titrating a Novispirin sample

with LTAC until the amide protons of Novispirin showed a satisfactory chemical shift dispersion (see Results). A 2D NOESY spectrum with 70 ms mixing time was recorded with a WATERGATE water suppression (*40*). [^{1}H,^{1}H]-TOCSY spectra with 40 and 80 ms mixing time, respectively, were recorded using the clean-TOCSY sequence (*41*) with a 15 kHz spin-lock and a WATERGATE water suppression. In addition, a 2QF-COSY experiment was recorded.

NMR experiments with LTAB were conducted at 25 °C, since higher temperatures led to a loss of amide proton signals, presumably due to fast chemical exchange with the solvent.

Detergent−Peptide Interactions. To investigate interactions between detergent and peptide, 2D NOESY spectra were recorded on samples with nondeuterated SDS and LTAC, but otherwise identical conditions as for the structure determination. In these spectra, the third (and last) 90° pulse was replaced by an off-resonance Q5 pulse (*39*) of 3.14 ms duration selectively exciting a region from 6 to 9 ppm. This leaves the magnetization of water and detergent nuclei in a longitudinal state thus minimizing the signal obtained from them. The remaining water signal was further suppressed by a WATERGATE element.

H^N Exchange. For the experiments determining the H^N exchange, the pH of the sample in SDS-d_{25} used for the structure determination was brought up to pH 5.7, which did not cause large changes in chemical shift. The sample of Novispirin in LTAB-d_{25} was used as for the structure determination. [^{1}H,^{1}H]-TOCSY spectra with 75 ms mixing time were recorded using the clean-TOCSY sequence (*41*) with a 15 kHz spin-lock and a WATERGATE water suppression. The sample of Novispirin in SDS-d_{25} was measured at 50 °C, the sample of Novispirin in LTAB-d_{25} at 25 °C. As a control, an identical TOCSY spectrum was recorded on a sample of 2.5 mM Novispirin at pH 5.7 containing 80 mM NaCl and 3 mM NaN_3 but no detergent. The control spectrum was recorded at 50 °C.

Diffusion Measurements. All diffusion measurements were performed at 17 °C to minimize convection in the sample tube.

1. SDS. The diffusion constant of Novispirin in SDS was measured by the convection-compensated, double-stimulated echo sequence (*44*). A diffusion delay of 100 ms was employed. Sine-shaped gradient pulses of 10 ms duration and 16 different, linearly spaced, strengths ranging from 2.4 to 48 Gcm^{-1} were used. Unlike the case of LTAB-d_{25}, there is no strong protonated signal available from SDS-d_{25}. Therefore, a sample of Novispirin in 284 mM SDS-d_{25} and 16 mM SDS was prepared for these measurements. The regions from 3 to 3.2 ppm (Novispirin arginine $H^{\delta 2,3}$) and 1.0−1.4 ppm (SDS 3-11-CH_2 with a minor contribution of Novispirin isoleucine $H^{\gamma 12}$) were integrated at each gradient strength. The latter signal contains contributions from both SDS and Novispirin ($H^{\gamma 12}$ of Ile side chains). Under these conditions (284 mM SDS-d_{25} with a degree of deuteration of 98%, 16 mM SDS, and 2.5 mM Novispirin), assuming 18 SDS H-atoms (3-11-CH_2) and 5 novispirin atoms ($H^{\gamma 12}$ of Ile side chains) to have their resonance in this area, the total contribution of the ^{1}H on SDS to this signal is 97%, while the Novispirin signals only contribute with 3%.

2. LTAC. Diffusion constants of Novispirin in solutions with increasing amounts of LTAC were measured by the convection-compensated, double-stimulated echo sequence (*44*).

A diffusion delay of 200 ms was employed. Sine-shaped gradient pulses of 4 ms duration and 16 different, linearly spaced, strengths ranging from 2.4 to 48 Gcm^{-1} were used. The signals at 6.76 ppm (Novispirin Y17 $H^{\epsilon 1,2}$) and 3.05 ppm (LTAC N−$(CH_3)_3$) were integrated at each gradient strength. Diffusion constants were obtained from the fitting routine in XWinNMR2.6 and 3.6.

Probing Micelle Penetration with Paramagnetic Reagents. For the experiments with the paramagnetic reagents a [^{1}H,^{1}H]-TOCSY spectrum with 20 ms mixing time was recorded using the clean-TOCSY sequence (*41*) with a 15 kHz spin-lock immediately before the addition of $MnCl_2$ (to a concentration of 0.5 mM for the sample with SDS and 4 mM for the sample with LTAB) and subsequent recording of an identical [^{1}H,^{1}H]-TOCSY spectrum. The mixing time was chosen in order to maximize the intensity of the H^N/H^α cross-peaks. The sample of Novispirin in SDS-d_{25} was measured at 50 °C, the sample of Novispirin in LTAB-d_{25} at 25 °C. Identical rectangular regions were integrated in both spectra, and the integral ratios were determined. Thirty rectangular regions in empty parts of the spectra were integrated, and a standard deviation of the integrals was determined. This was assumed to be the error of the integration. The error of the ratio was determined from the errors of the single values as outlined in ref *45*.

1. Structure Calculation. NOE cross-peaks were identified, integrated, and assigned in the aforementioned NOESY spectra using the program XEASY (*43*) and the NEASY subroutine of CARA (*46*). Backbone torsion angle restraints were obtained from secondary chemical shifts using the program TALOS (*47*). TALOS-derived angle constraints were only accepted for residues, where all the 10 best database hits were situated within the same region of the Ramachandran plot. A deviation from the TALOS-derived value of ±30° was allowed. The CALIBA (*48*) subroutine in CYANA was used to convert cross-peak intensities from NOESY spectra into distance constraints. The CYANA subroutine FOUND (*49*) was used to add angle restraints. On the basis of this input, the structure was calculated using the torsion angle dynamics program CYANA (*50*). Structure calculations were started from 100 conformers with random torsion angle values. The 20 conformers with the lowest final CYANA target function values were embedded in a water shell of 8 Å thickness and energy-minimized against the AMBER force field (*51*) with the program OPALp (*52*).

No further refinement was performed. The structures were checked by PROCHECK_NMR (*53*).

Viscosity Measurements. LTAC micellar diffusion constants were calculated according to the following equation:

$$D_{\mathrm{mic}} = \frac{D_{\mathrm{observed}} - \frac{\mathrm{cmc}}{c} D_{\mathrm{monomer}}}{1 - \frac{\mathrm{cmc}}{c}} \qquad (3)$$

where D_{observed} is the measured diffusion constant of LTAC, D_{monomer} is the diffusion constant for monomeric LTAC, c is the concentration of LTAC, and cmc is the critical micelle concentration (13 mM). Diffusion constants are converted to hydrodynamic radii by help of the Stokes−Einstein

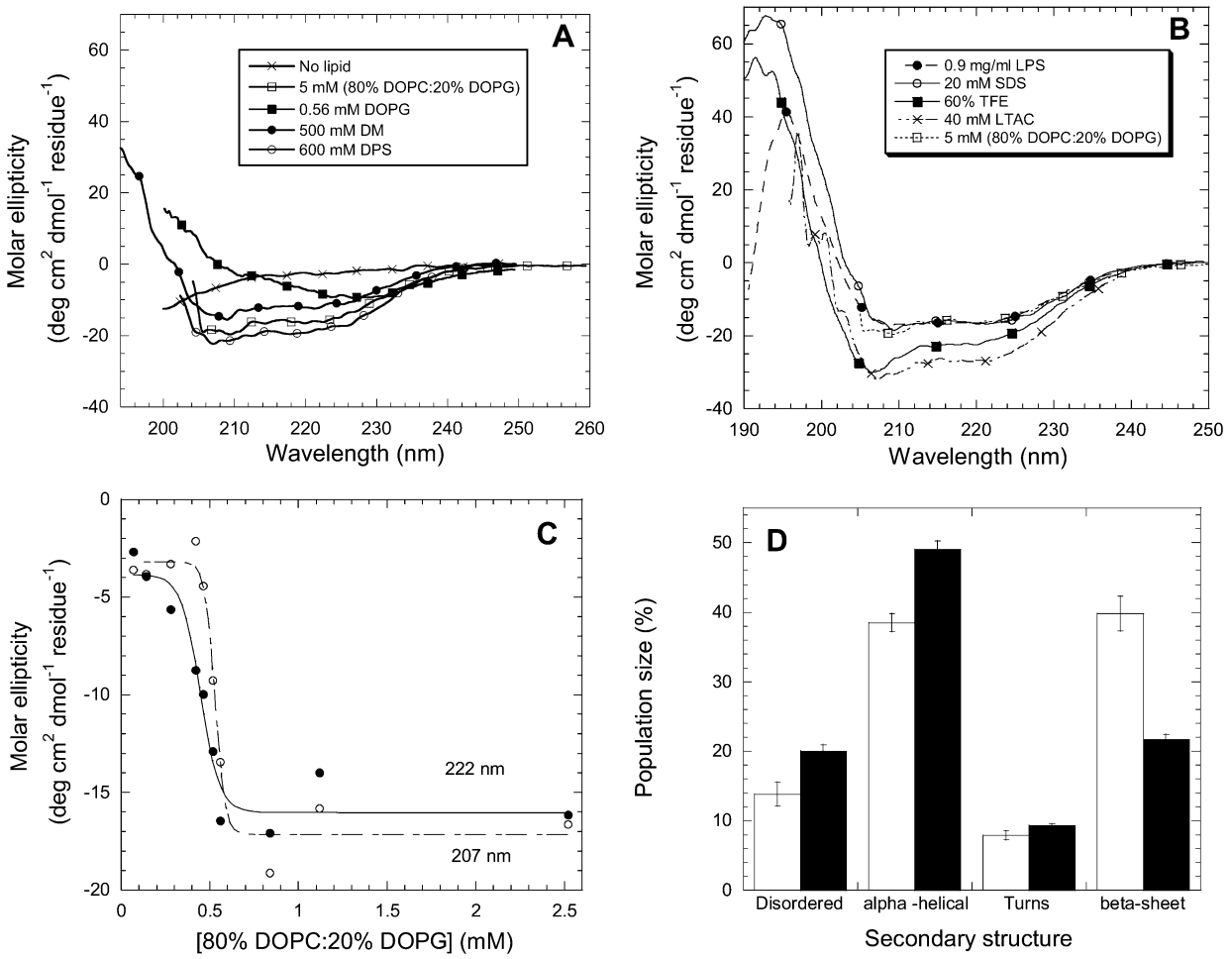

FIGURE 1: (A and B) Representative far-UV CD spectra of Novispirin in different amphiphilic environments. The spectrum in 80% DOPC/20% DOPG is shown in both spectra for ease of comparison. (C) Molar ellipticities of Novispirin at 222 and 207 nm as a function of the concentration of the lipid mixture 80% DOPC/20% DOPG. Data fitted to eq 1 (as shown in Table 2). (D) Secondary structure of the Novispirin aggregates formed in 1 mM DOPG (white columns) or 0.75 mM SDS (black column).

equation to account for changes in sample viscosity at different detergent concentrations:

$$R_h = \frac{kT}{6\pi\eta D} \quad (4)$$

where R_h is the hydrodynamic radius, k is the Boltzmann constant, T is the absolute temperature, η is the kinematic viscosity of the solution, and D is the diffusion constant.

The kinematic viscosity of aqueous solutions of LTAC (0 M $\leq$ [LTAC] $\leq$ 1 M) was determined by a Brookfield Digital Viscosimeter DV-II with a UL adapter. Over the interval 0−1 M, the viscosity of LTAC solutions could be fitted to a quadratic curve (data not shown):

$$\eta(c_{LTAC}) = 1.13 + 1.23c_{LTAC} + 1.04c_{LTAC}^2 \quad (5)$$

RESULTS

Importance of Electrostatic Interactions in Novispirin−Lipid Interactions. The first objective of this study was to compare the ability of lipids and detergents to induce the α-helical structure observed for Novispirin in TFE (*30*). This process is followed by far-UV CD spectroscopy. A representative overview of far-UV CD spectra of Novispirin in different amphiphiles and TFE is shown in Figure 1A,B. We start by determining optimal conditions for lipid interactions. In buffer alone, Novispirin only has a weak signal in the far-UV CD spectrum (Figure 1A), indicative of a very low degree of organized structure. Pure zwitterionic DOPC lipid vesicles do not lead to an appreciable increase in Novispirin structure. This is not surprising, as Novispirin has a net charge of +7 at pH 7.5 and would be expected to require negatively charged lipids to bind to vesicles. Nevertheless, vesicles with 10% DOPG do not alter the Novispirin structure compared to DOPC alone. However, this changes as we increase the fraction of anionic lipid. Vesicles containing 20−80% DOPG all show similar spectra with minima at 222 and 209 nm, which are typical of α-helical structure (cf. spectra shown in Figure 1A). There is a cooperative increase in CD signal between 0.5 and 1 mM lipid, after which it reaches a plateau level (shown in Figure 1C for the lipid mixture containing 80% DOPC and 20% DOPG and summarized in Table 1), corresponding to essentially 100% α-helix, according to the deconvolution program Continell (*54*). There is no isodichroic point (data not shown), suggesting that the transition involves more than two states. Thus, the signal changes at the two minima, 207 and 222 nm, though similar, do not coincide completely when plotted versus lipid concentration (Figure 1C). Note the cooperative nature of the transition.

In 100% DOPG, Novispirin forms visible aggregates and the corresponding CD spectrum is significantly altered

Table 1: Cooperative Unfolding Parameters for Novispirin in Different Environments

amphiphile	concentration units	wavelength (nm)	c^a	$L_{50\%}{}^b$
20% DOPC, 80% DOPG	mM	207	15.5 ± 4.9	0.53 ± 0.01
20% DOPC, 80% DOPG	mM	222	8.0 ± 3.2	0.45 ± 0.02
TFE	% (v/v)	222	0.12 ± 0.04	16.6 ± 1.5
TFE	% (v/v)	207	0.13 ± 0.06	17.7 ± 0.4
TFE	% (v/v)	190	0.11 ± 0.04	18.0 ± 060
SDS	mM	222	1.33 ± 0.36	0.98 ± 0.09
SDS	mM	207	4.8 ± 4.3	1.94 ± 0.09
SDS	mM	190	0.68 ± 0.25	1.31 ± 0.17

[a] The cooperativity constant (eq 2). The lower *c* is, the more gradual the transition. [b] The concentration at which the binding transition is halfway to completion (eq 2).

(Figure 1A). This structural change already occurs at low DOPG concentrations, after which no further change is seen (data not shown). Due to light-scattering artifacts, CD is not appropriate to analyze protein aggregates. However, an analysis of the aggregated state by FTIR shows that the α-helix content is reduced to around 50% with a compensating rise in β-sheet and turns (Figure 1D). FTIR analysis of Novispirin in solution with SDS shows very little or no β-structure (data not shown). Interestingly, the CD spectrum in DOPG is very similar to that of Novispirin in *E. coli* total lipid extract, which contains around 60% PE lipids and 18% PG lipids (data not shown). PE lipids do not appear to play a large role in this structure-induction, since synthetic DOPC lipids containing 10−20% DOPE showed no increase in Novispirin structure compared to pure DOPC (data not shown).

The strong effect of including DOPG clearly indicates electrostatic interactions between Novispirin and lipids. This is confirmed by the screening effect of high ionic strength. In 200 mM NaCl, lipids containing 20% DOPG are unable to induce α-helical structure in Novispirin, whose far-UV CD spectrum under these conditions is identical to that in buffer (data not shown).

Different Modes of Binding of Novispirin to LPS and TFE. Previously, it has been shown that components of the cell wall of Gram-negative and Gram-positive bacteria, namely, lipopolysaccharides from *Pseudomonas aeruginosa* and lipoteichoic acid from *Staphylococcus aureus*, respectively, are able to induce α-helical structure in Novispirin at 1 mg/mL (*30*). However, it is not clear whether this concentration is sufficient to saturate the level of helicity. A more quantitative analysis of the interaction using 0−0.9 mg/mL LPS from *E. coli* EH100 (spectrum shown in Figure 1B) leads to an isodichroic point around 203 nm, suggesting a simple two-state binding-and-folding model (data not shown). Fitting the data to this model using three different wavelengths (eq 1 and Figure 2A) leads to an apparent K_d of 0.7−1.1 mg/mL, indicating that the structural transition is around 60% complete at 1 mg/mL (Table 2). The cmc of LPS is in the low μg/mL range (*55*), indicating that the interactions with Novispirin only involve LPS micelles. It is noteworthy that the affinity of LPS for Novispirin is comparable to that of DOPC/DOPG vesicles; in both cases, the transition nears completion around 1 mg/mL LPS or lipid.

For similar quantitative reasons, we titrated Novispirin with TFE. TFE (33−40%) has been shown to be sufficient to lead to α-helix formation in Novispirin (*30*). The spectra between 0 and 60% TFE reveal a very clear isodichroic point around 202 nm (data not shown; spectrum in 60% TFE shown in Figure 1B) with a cooperative change in the CD signal at different wavelengths (Figure 2B). A plateau is reached around 30% TFE with a midpoint around 16−18% (Table 1), indicating that 33−40% TFE is an appropriate condition for analyzing the NMR structure of Novispirin.

Effect of SDS on Novispirin. The interaction of Novispirin with detergents is interesting, since these substances are lipid-mimetic but more amenable to studies by NMR. Of these, SDS is particularly appropriate due to its well-documented ability to induce α-helical structure. SDS also induces clear α-helical structure in Novispirin in the low millimolar range (Figure 1B). While the 190 and 222 nm data reveal a cooperative transition which can be fitted to eq 2, the data at 207 nm can be divided into three regions, namely, a plateau around 0−0.5 mM, followed by a rather abrupt jump to another plateau between 0.5 and 1.4 mM SDS, leading via a broader transition to a plateau above ca. 2.4 mM (Figure 2C). The midpoint of around 1 mM is only about twice as high as for the vesicles with the highest affinity for Novispirin, namely, 20% DOPC and 80% DOPG (Table 1). Since the cmc of SDS is 2.4 mM under our buffer conditions (20 mM NaP, pH 7.5), SDS is predominantly monomeric in all these regions. There is visible precipitation in the plateau region between 0.5 and 1.4 mM SDS (where the [SDS]/[Novispirin] goes from 12 to 35), confirmed in Figure 2D where it was possible to spin down most of the protein in this detergent range. An FTIR analysis revealed that the α-helix content had decreased to around 40% together with a similar amount of β-sheet as well as some turns and disordered structure (Figure 1D). This contrasts with an α-helical content close to 100% at higher SDS concentrations where Novispirin is soluble.

Unlike the case for lipids, the interaction between Novispirin and SDS must involve hydrophobic as well as electrostatic interactions, since addition of up to 500 mM NaCl had no significant effect (data not shown).

Neutral and Zwitterionic Detergents Induce Structure at Higher Concentrations. Interestingly, the neutral detergent dodecyl maltoside as well as the zwitterionic detergent DPS (3-(dodecyldimethylammonio)propane sulfonate) induce α-helical structure, although this requires much higher detergent concentrations than SDS. Both detergents show dichroic points around 204 nm (data not shown; representative spectra shown in Figure 1A), and the solutions show no visible precipitation. Data follow a hyperbolic binding curve with a midpoint around 140−210 nm (DM, Figure 3A) or 82−120 mM (DPS, Figure 3B), which is around 100−200 times as high as for SDS, as well as being high above the cmc of these detergents (0.17 and 4 mM for DM and DPS, respectively).

Ability of LTAC To Induce Structure in Novispirin and Role of Electrostatics. Remarkably, the cationic detergent LTAC clearly induces α-helical structure in Novispirin (Figure 1B), even under conditions where there is a high positive charge on the peptide. At pH 7.5 (overall charge: ca. +7), salt reduces the binding and α-helical folding of Novispirin, but at pH 11 (overall charge ca. +2), salt does not have any significant effect. Helix formation occurs earlier in the presence of salt at pH 11, but this partly reflects NaCl's

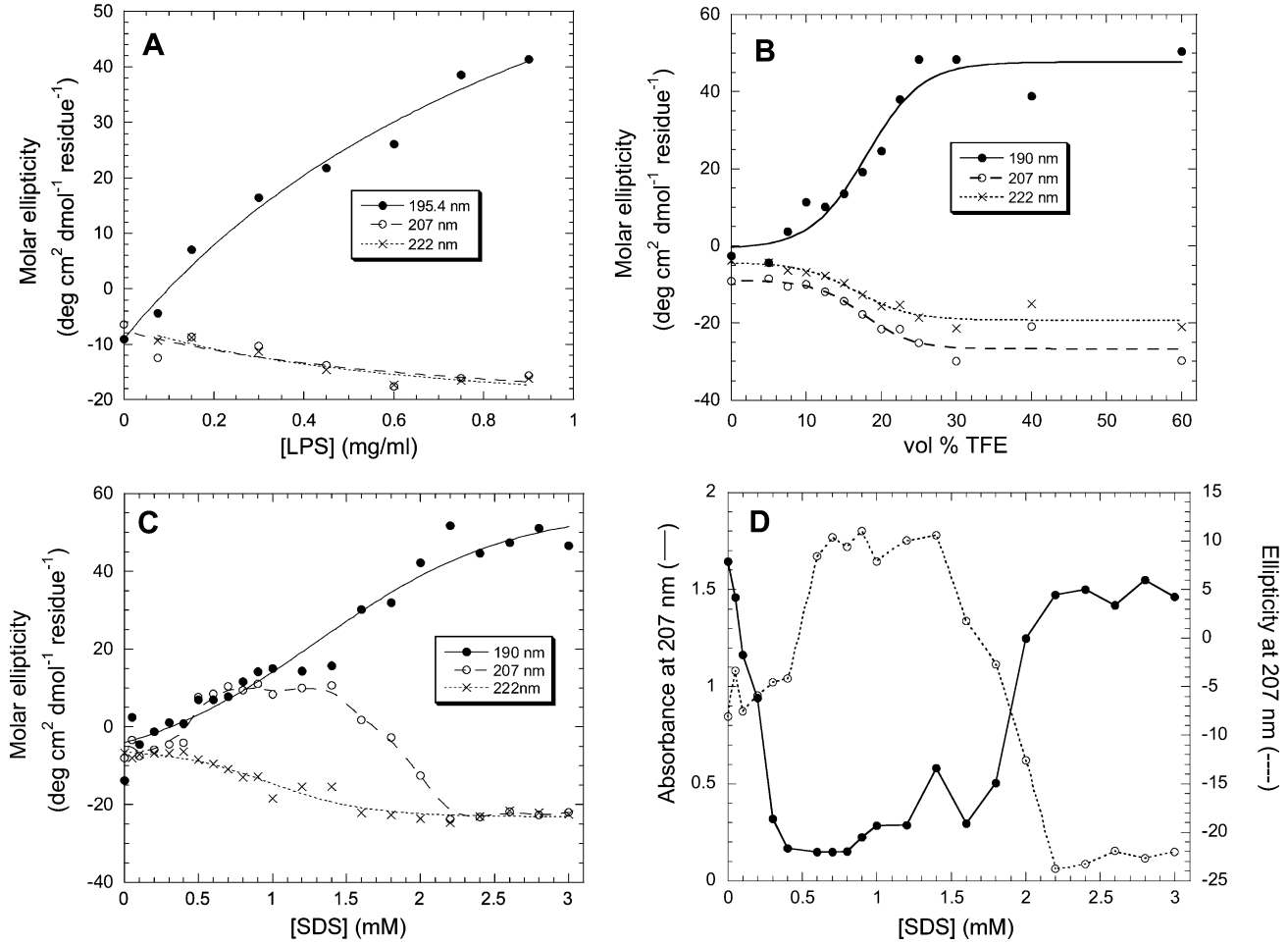

FIGURE 2: (A) Molar ellipticity of 40 μM Novispirin as a function of lipopolysaccharide from *E. coli*. Data fitted to eq 1 (results in Table 3). (B) Molar ellipticity of 40 μM Novispirin as a function of TFE. Data fitted to eq 2. (C) Molar ellipticity of 40 μM Novispirin as a function of SDS. Data for 190 and 222 nm are fitted to eq 2, while data at 207 nm are joined up for clarity. Data are restricted to 0−3 mM for clarity; there are no further transitions beyond 3 mM SDS. Increasing the Novispirin concentration to 400 and 1140 μM leads qualitatively to the same transitions, although the spectral changes occur later at higher SDS concentrations. (D) Solubility of 40 μM Novispirin as a function of SDS concentration. Novispirin was incubated at different SDS concentrations and centrifuged, and the absorbance (joined lines) and ellipticity at 207 nm (stippled lines) of the supernatant were measured.

Table 2: K_d Values for Binding of Novispirin to Detergents Showing Hyperbolic Unfolding Curves[a]

wavelength	LPS (mg/mL)	DM (mM)	DPS (mM)
222	0.67 ± 0.94	190 ± 50	120 ± 20
207	0.80 ± 0.90	210 ± 160	110 ± 25
190 (195.4)	1.15 ± 0.60	140 ± 30	82 ± 22

[a] K_d is defined in eq 1.

reduction of LTAC's cmc due to its ability to reduce electrostatic repulsion between headgroups (Figure 3C, Table 3). As seen for the zwitterionic and nonionic detergents, there is a dichroic point and no precipitation (data not shown).

NMR Assignment and Structure Calculation. A comparison of the far-UV CD spectra of Novispirin in different detergents and solvents reveals that, although the same overall helical structure is observed, there are subtle changes in the distribution of minima (Figure 1B). The spectra in SDS, LPS, and lipid fall in one class, whereas those in LTAC and TFE fall into their own separate classes. Since only the structure of Novispirin in TFE is known in any detail, we have determined the structure of Novispirin in deuterated SDS and LTAB to analyze the effect of detergents on Novispirin structure in more detail. Note that LTAB was only used for NMR experiments that require deuterated detergents, due to the availability of the deuterated form; for all other experiments, LTAC was used because of the prohibitively high absorption of LTAB in the far-UV area.

The concentration of LTAC necessary for helix formation strongly depends on the pH. The presence or absence of secondary structure can be assessed from the H^N region of a ^{1}H NMR spectrum. A high dispersion of chemical shifts as found in the spectrum of Novispirin in 1030 mM LTAC at pH 5.7 (Figure 4) is indicative of the presence of secondary structure, while a low dispersion of chemical shifts as found in the spectrum of Novispirin at pH 5.7 in the absence of LTAC (Figure 4) points at a random-coil structure. The NMR spectrum of Novispirin in 270 mM LTAC at pH 7.5 clearly indicates the presence of secondary structure. This structure is lost upon titration toward the acidic range (Figure 4 and CD, data not shown). This loss of secondary structure can, however, be reversed by adding larger quantities of LTAC (Figure 3C and Figure 4). We therefore chose pH 5.7 and 1030 mM LTAB-d_{25} as suitable conditions for determining Novispirin's structure by NMR.

In SDS, Novispirin retains the same helix-rich CD signal down to pH 3 unaltered (data not shown). NMR analysis

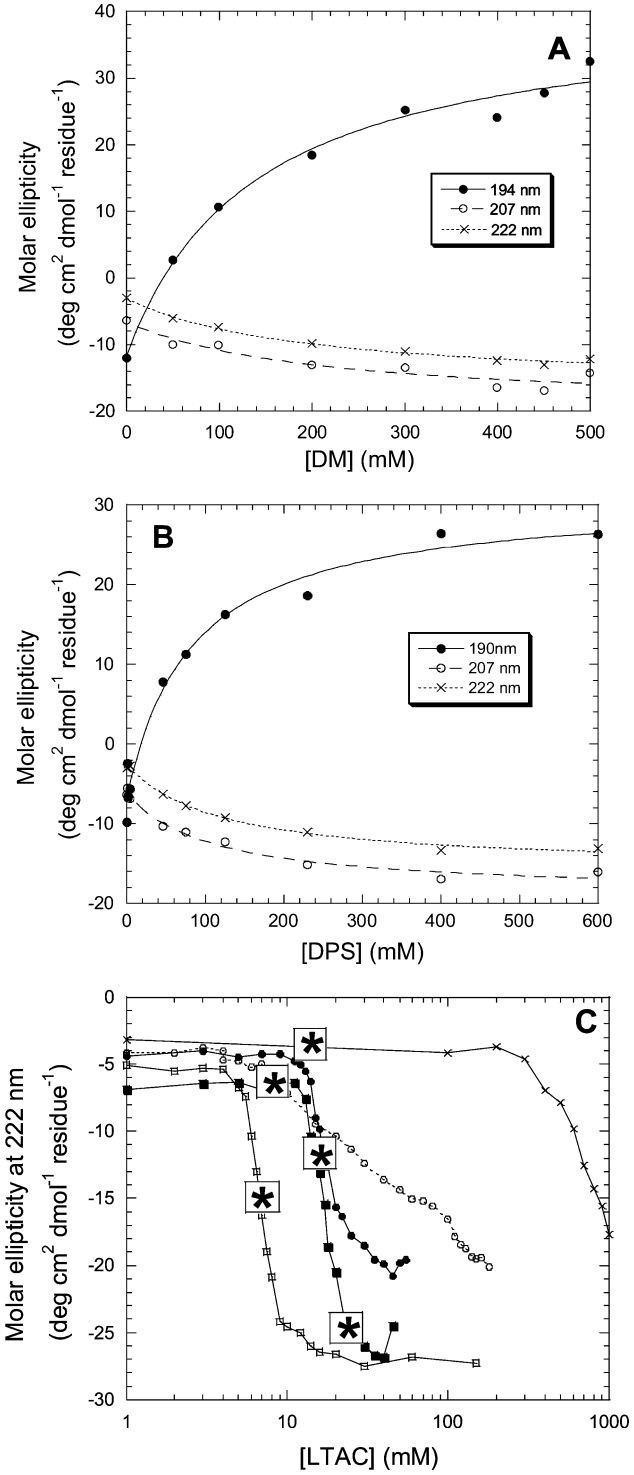

FIGURE 3: (A) Molar ellipticity of Novispirin as a function of DM. Data fitted to eq 1. (B) Molar ellipticity of Novispirin as a function of DPS. Data fitted to eq 1. (C) Titration of Novispirin with LTAC under different conditions: pH 5.7, 0 mM NaCl (×); pH 7.5, 0 mM NaCl (●); pH 7.5, 200 mM NaCl (○); pH 11, 0 mM NaCl (■); pH 11, 200 mM NaCl (□). Asterisks indicate cmc of LTAC under the various experimental conditions. Note the logarithmic scale.

was carried out at pH 4.7. The ^{1}H atoms of Novispirin in SDS could be assigned with the following exceptions: K1 (all protons), N2 H^N, K9, K15, and K16 side-chain atoms (H^β,H^γ,H^δ,H^ϵ,H^ζ). All lysine signals were extremely weak; some lysine side-chain signals could be found but not unambiguously assigned. A set of 20 structures was calculated. Table 4 lists some quality criteria for the structure. The structure shows two well-defined helical regions, whose orientation toward each other was not defined (see Figure 5A). The first helix stretches approximately from residue 2 to 9, the second helix from residue 12 to 17. Residues 10 and 11 form a hinge. From the sequence plot (Figure 6A), it can be seen that helix 1 is well-defined with many $d_{\alpha N(i,i+3)}$

Table 3: Interactions between Novispirin and LTAC at Different pH Values and Ionic Strengths

pH	[NaCl] (mM)	CMC [mM]	C^a	$L_{50\%}{}^a$ (mM)	$[\theta]_{end}$ (deg cm^2 dmol^{-1} residue^{-1})
5.7	0	14.3	—[b]	—[b]	—[b]
7.5	0	16.8	0.17 ± 0.02	17.3 ± 0.3	−19.5 ± 0.3
7.5	200	8.4	(low)	40.5 ± 4	−23.5 ± 0.5
11	0	23	0.20 ± 0.02	17.3 ± 0.2	−25.8 ± 0.3
11	200	7	0.49 ± 0.03	7.0 ± 0.07	−26.4 ± 0.2

[a] Defined in legend to Table 1 and eq 2. [b] Transition not complete.

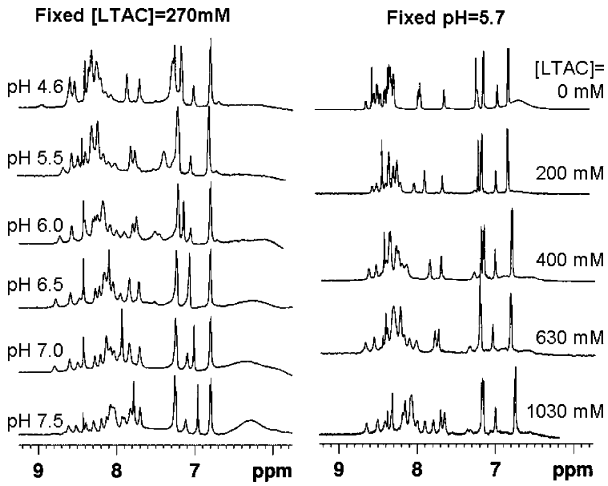

FIGURE 4: H^N/aromatic region of the ^{1}H NMR spectrum of Novispirin. Left panel: constant 270 mM of LTAC, decreasing pH. Right panel: constant pH 5.7, increasing concentrations of LTAC. The spectra were obtained using excitation-sculpting water suppression (*38*) and a selective Q5 pulse of 3.14 ms duration exciting only the region from 6 to 9 ppm.

Table 4: Quality Criteria for the Calculated Novispirin Structures

detergent	SDS	LTAB
number of distance constraints	168	131
- of which intraresidual	96	77
- of which sequential	37	35
- of which medium-range ($2 \le \Delta_{res} \le 4$)	35	19
number of angle constraints[a]	20	18
- of which ϕ	10	9
ψ	10	9
CYANA residual target function	1.0 ± 0.05 Å^2	0.11 ± 0.02 Å^2
distance restraints violated by more than 0.2 Å[b]	0	0
angle restraints violated by more than 5°[b]	0	0
backbone rmsd values residues 2−9[c]	0.66 ± 0.25	0.30 ± 0.09
backbone rmsd values residues 12−17[c]	0.37 ± 0.12	0.23 ± 0.14
Ramachandran plot[d]		
% of residues in most favored regions	78.3%	76%
% of residues in less favored regions	20.3%	22.5%
% of residues in generously allowed regions	1.4%	—
% of residues in disallowed regions	—	1.5%

[a] Only those derived by TALOS (*47*). [b] Per molecule. [c] As calculated by MOLMOL (*64*) from the pairwise rmsd values of each of the 20 structures against a mean structure. [d] As calculated by PROCHECK_NMR (*53*) excluding Gly residues.

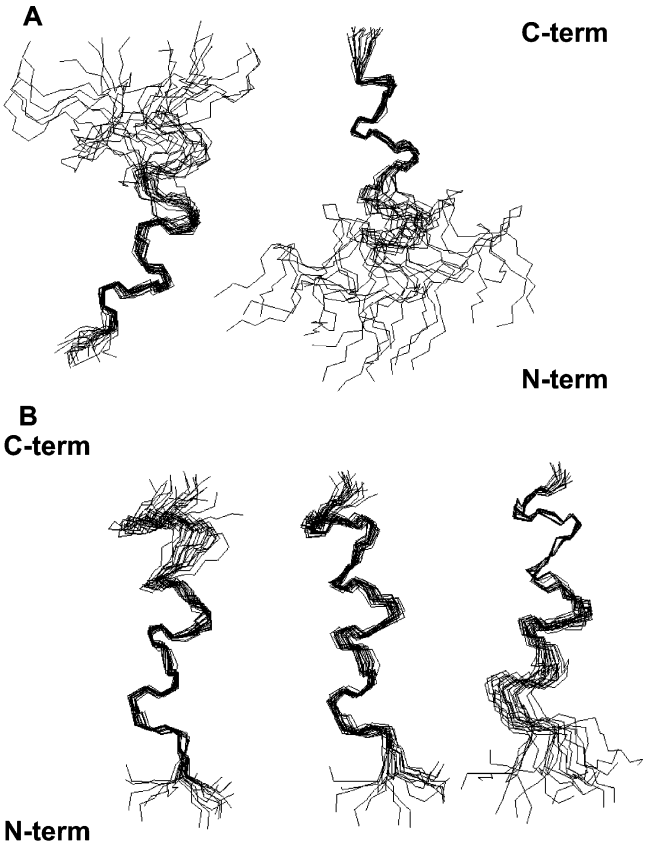

FIGURE 5: Structure of Novispirin in the presence of (A) SDS and (B) LTAB. The aligned bundle of the 20 structures with the lowest residual target function is shown. In the left panel, N, C, and C^{α} atoms of residues 2−9 are aligned; in the right panel, N, C, and C^{α} atoms of residues 12−17 are aligned. In the case of LTAB, a central panel with an alignment of N, C, and C^{α} atoms of residues 2−17 (i.e., the combination of the helical two regions) is also included.

cross-peaks, whereas helix 2 is only defined by relatively few cross-peaks. However, in addition to those shown in the sequence plot, there are interactions between the aromatic ring protons of Tyr 17 and the side chain of Ile 14. This is also reflected in atypical chemical shifts of the side-chain protons of Ile 14. The helicity of these regions is also corroborated by strong sequential H^N-H^N NOEs. At present, we are unable to decide whether the lack of structural information around residue 12 actually reflects mobility or is caused by an artifact (e.g., lack of NMR signals in this region).

In LTAB, the ^1H atoms of Novispirin could be assigned with the following exceptions: K1 (all protons) and N2 H^N. Quality criteria are listed in Table 4. As in SDS micelles, the structure shows 2 helical stretches, but in contrast to the structure in SDS, the kink between the two helices is well-defined and the whole structure (Figure 5B) can be aligned simultaneously. The sequence plot (Figure 6B) clearly shows the presence of two helical stretches.

Micelle Penetration Investigated by Paramagnetic Reagents. In addition to obtaining the structure of Novispirin, it is of interest to investigate to which extent the peptide is buried in the micellar environment or exposed to the surroundings. We have used four complementary techniques to obtain more information on this, namely, quenching of signals by paramagnetic reagents, NOEs between peptide and

FIGURE 6: Sequence plot of Novispirin NMR data (A) for Novispirin in SDS at 50 °C and (B) for Novispirin in LTAB at 25 °C. The sequential NOE connectivities $d_{\alpha N}$, d_{NN}, and $d_{\beta N}$ are indicated with black bars of a thickness that corresponds to the strength of the NOEs. The medium range connectivities $d_{\alpha N}(i,i+3)$ and $d_{\alpha\beta}(i,i+3)$ are shown by lines starting and ending at the positions of the residues related by the NOE. Residues whose ϕ and ψ angles were constrained based on output from TALOS are underlined. The line CSI gives the chemical shift index. A "+" indicates that the chemical shift of the H^{α} is larger than the random-coil chemical shift +0.1 ppm; a "-" indicates a H^{α} chemical shift lower than the random-coil chemical shift −0.1 ppm. A "0" indicates a shift that is within 0.1 ppm from the random-coil value. Random-coil values were taken from ref *40*.

Table 5: NOESY Cross-Peaks Found between SDS and Novispirin[a]

	SDS-atom				
Novispirin	1-CH_2	2-CH_2	3-CH_2	4−11-CH_2	12-CH_3
R4/R5[b] H^{ϵ}		?		x	
R8 H^{ϵ}		?	x	x	
H12 $H^{\delta 2}$		?	x	x	
H12 $H^{\epsilon 1}$		?		x	
Y17 $H^{\delta 1,2}$			x	x	
Y17 $H^{\epsilon 1,2}$		x	?	x	

[a] Peaks are denoted with an "x". A "?" denotes cases where neither the absence nor the presence of the peak can be proven unambiguously because of spectral overlap with other cross-peaks. [b] The H^{ϵ} of R4 and R5 have the same chemical shift; the cross-peak can, therefore, not be assigned to only one of the two atoms.

detergent, PFG-diffusion measurements, and finally H^N exchange.

Paramagnetic reagents such as Mn^{2+} are useful probes of the solvent-accessibility of different parts of a protein or peptide (*56*). When Mn^{2+} ions come into close proximity with protons, their nuclear magnetic relaxation will be enhanced, leading to signal broadening.

1. SDS. Upon addition of 500 μM $MnCl_2$, several signals of Novispirin were weakened or vanished altogether, whereas others were affected much less. Table 5 and Figure 7 show the results of these experiments. Because of electrostatic interactions, it is assumed that most of the Mn^{2+} is localized on the negatively charged surface of the SDS micelles. The presence of Mn^{2+} ions has only little effect on resonances

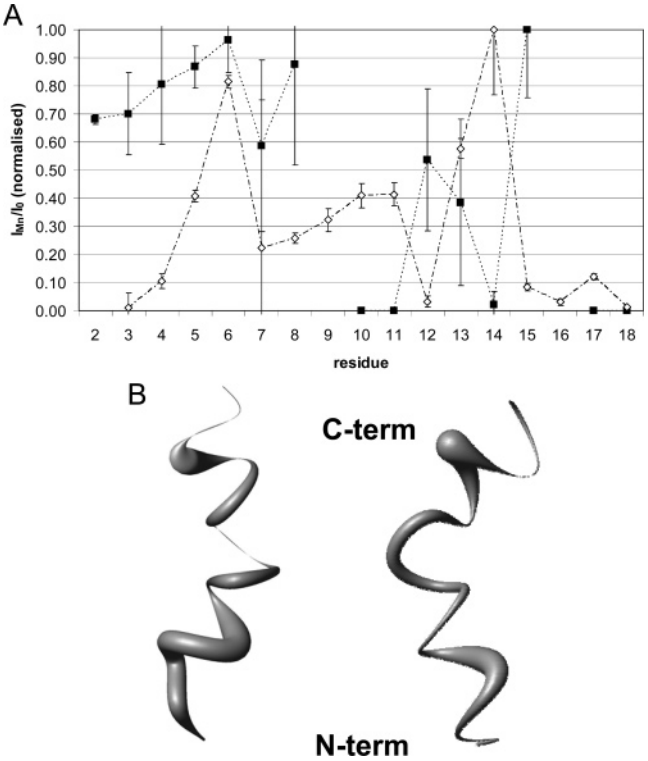

FIGURE 7: (A) Influence of paramagnetic Mn^{2+} ions on relative signal intensity of Novispirin in SDS at 50 °C (closed squares) and LTAB at 25 °C (open diamonds). The top graph shows I_{Mn}/I_0 plotted vs the peptide sequence, where I_{Mn} is the signal intensity in a clean-TOCSY spectrum (*41*) of 20 ms mixing time with a 15 kHz spin-lock and a WATERGATE water suppression (*40*) after addition of 0.5 mM Mn^{2+}, and I_0 is the signal intensity before addition of Mn^{2+}. The highest ratio occurring in each of the samples was normalized to 1, since no comparisons of absolute signal intensity between two different samples could be made. In general, signal intensity ratios are far weaker for LTAB than for SDS. (B) Visualization of the data using the structures for Novispirin in SDS (left) and LTAC (right). The backbone is represented by a spline function, whose radius is proportional to the I_{Mn}/I_0 value plotted in the top graph. The thinner the curve, the more this individual residue is influenced by Mn^{2+} ions.

of residues 2−6 and 8 forming the first helix. A medium effect on residue 7 could be observed. Data on residue 9 have been omitted due to a standard error of more than 100%. Resonances from residues 10 and 11 have disappeared completely, and a moderate effect of the Mn^{2+} ions on residues 12 and 13 can be observed. The resonance of residue 14 has vanished, while that of residue 15 is not affected at all. No data can be obtained on residue 16, and the resonances of the last two residues, 17 and 18, vanish upon addition of Mn^{2+}.

2. LTAB. Upon addition of 4 mM $MnCl_2$, most Novispirin signals diminished or vanished altogether. The fact that a much larger Mn^{2+} concentration was needed to observe an effect compared to SDS micelles is ascribed to the charge of the micellar surface that attracts Mn^{2+} ions in the case of SDS but repels them in the case of LTAB. The data are presented in Table 5 and Figure 7. The only H^N/H^α signals remaining are those of the hydrophobic residues Ile 6, Ile 13, and Ile 14. The signals of the aromatic protons of Tyr 17 remain visible, although its H^N/H^α cross-peak does not.

NOEs between Detergent and Novispirin Molecules. 1. SDS. The 2D-selective NOESY spectrum revealed several cross-peaks from Novispirin side-chain atoms to SDS atoms. The found cross-peaks are summarized in Table 5. No cross-peaks were found from backbone H^N atoms of Novispirin to SDS atoms. Because of severe spectral overlap, only side-chain atoms with a chemical shift >5.5 ppm could be investigated. Neither the presence nor the absence of NOEs between other side-chain atoms, notably Ile and Leu methyl groups, and SDS can be proven. In addition to the cross-peaks given in Table 5, a number of cross-peaks were found that could not be assigned to any peptide atom. They could possibly belong to Lys H^ζ atoms, but as none of them are assigned, this cannot be confirmed.

2. LTAC. No NOEs between any Novispirin atom with a chemical shift >5.5 ppm and LTAC atoms could be detected. NOEs between other Novispirin side-chain atoms and LTAC cannot be ruled out, but they cannot be observed due to spectral overlap.

H^N Exchange in SDS and LTAB. Figure 8 shows the H^N/H^α regions of TOCSY spectra with 75 ms mixing time obtained from Novispirin in SDS, in LTAB, and in the absence of detergents, all at pH 5.7. Although Novispirin in SDS was measured at 50 °C while Novispirin in LTAB was measured at 25 °C, there are numerous H^N/H_2O exchange peaks in the LTAB solution and only a few in the SDS solution. The latter can be attributed to exchangeable arginine side-chain atoms, while not a single H^N exhibits exchange. In LTAB, there is more exchange—only Ile 6, Ile 13, Ile 14, Lys 16, Tyr 17, and Gly 18 H^N definitely do not yield an exchange peak. A control experiment with Novispirin at pH 5.7 and 50 °C in the absence of detergent showed strong backbone H^N exchange. The F2-rows of the TOCSY spectra are shown along with the 1D NMR spectra to demonstrate that the cross-peaks originate from chemical exchange and not from a combination of F1-ridges and insufficient water suppression. Weak examples for the latter can be seen but are having opposite sign to the "true" exchange peaks in the spectra of Novispirin in both detergents.

Novispirin−Micelle Association Probed by PFG Diffusion Experiments. The results of the previous three techniques make it reasonable to infer that Novispirin, at least in part, is buried in the SDS micelle, whereas it is questionable whether Novispirin is at all associated with LTAC micelles (see Discussion). Measurement of the diffusion constant for Novispirin could provide more insight. In the case of SDS, diffusion constants obtained from Novispirin and SDS are equal within the accuracy of the measurement. Under the conditions mentioned above, the diffusion constant for both Novispirin and SDS is 0.11×10^{-10} m^2 s^{-1}, where free Novispirin in water diffuses with 1.75×10^{-10} m^2 s^{-1}. The contribution of monomeric SDS to the measured diffusion constants is negligible at the high salt concentrations used. The diffusion constants obtained from Novispirin and LTAC with increasing amounts of LTAC present are given in Table 6. They show that the diffusion constant of Novispirin drops with increasing LTAC concentration. This is converted to hydrodynamic radius using the Stokes−Einstein equation (eq 4), which also takes into account changes in the viscosity of the solution with increasing LTAC concentration (see Materials and Methods). Diffusion constants of LTAC micelles are higher than those of SDS micelles, which is in agreement with the fact that SDS micelles are larger than LTAC micelles (*57*).

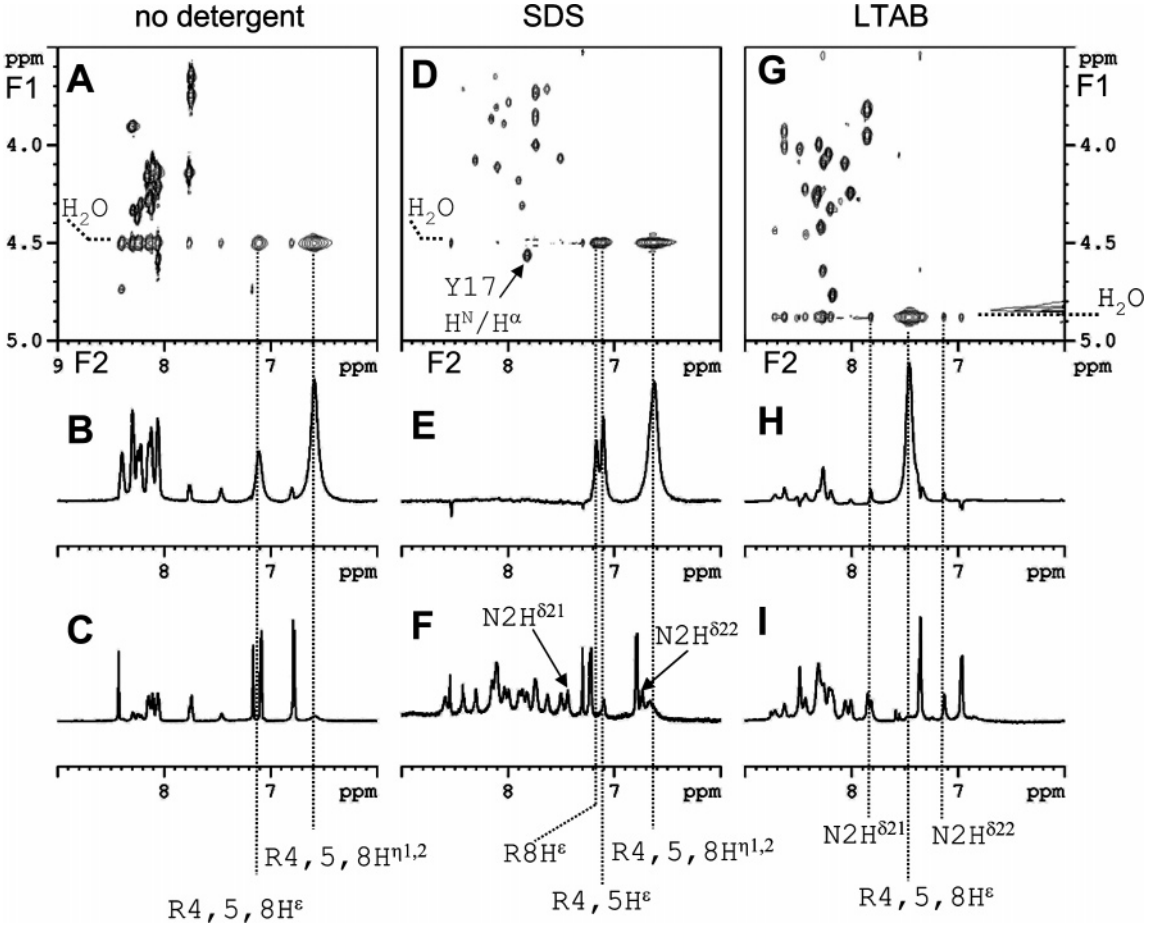

FIGURE 8: H^N/H^α regions of TOCSY spectra with 75 ms mixing time of Novispirin in (A) the absence of detergent, (D) SDS, and (G) LTAB micelles. The spectra were recorded using the clean-TOCSY sequence (*41*) with a 15 kHz spin-lock and a WATERGATE water suppression (*40*) with selective pulses. The chemical shift of water is 4.76 ppm in the spectrum of Novispirin in LTAB (recorded at 25 °C) and 4.50 ppm in the spectra recorded in the presence of SDS and in the absence of detergents (recorded at 50 °C), respectively. The F2-rows of the TOCSY spectrum at the chemical shift of water are presented (B) in the absence of detergent, (E) in SDS micelles, and (H) in LTAB micelles. The bottom line shows 1D NMR spectra recorded using excitation-sculpting water suppression (*38*) and selective excitation of the region from 6 to 9 ppm by an off-resonance Q5 pulse (*39*) of 3.14 ms duration. Spectrum C is from Novispirin in the absence of detergents, spectrum F from Novispirin in SDS, and spectrum I from Novispirin in LTAB.

The hydrodynamic radii of LTAC and Novispirin versus LTAC concentration are plotted in Figure 9. The data show that the apparent hydrodynamic radius of Novispirin remains essentially unchanged up to approximately 630 mM, after which it begins to increase. This is in contrast to the NMR spectra measured at different concentrations of LTAC (Figure 4) which already show signs of chemical shift dispersion of H^N atoms, pointing at the formation of stable secondary structure elements at LTAC concentrations as low as 200 mM. We interpret the data as a sign of beginning secondary structure formation, as detergent concentrations increase, maybe aided by transient interactions with the LTAC micelles. However, the association/dissociation equilibrium at low LTAC concentrations is still shifted toward the free form of Novispirin.

DISCUSSION

In the present work, we have investigated the influence of different detergents and lipids as well as TFE on the secondary structure of Novispirin G-10. For two detergents, SDS and LTAB, we have determined the structures of the peptide by solution-state NMR and obtained information on how the peptide is oriented relative to the detergent micelle.

Different Binding Modes of Novispirin. The titration of Novispirin with different additives clearly follows different binding modes. For lipids, TFE, SDS, and LTAC, there is a cooperative transition, while LPS and the detergents DM and DPS elicit a hyperbolic binding curve. Hyperbolic binding occurs well above the cmc of the detergents in all three cases, suggesting a simple equilibrium between free and micelle-bound peptide. TFE's cooperative transition is a simple consequence of a linear relationship between the free energy of folding and TFE concentration (*31*), similar to that seen for denaturants (*58*). In the case of SDS, the cooperative binding is completed below bulk cmc, and this indicates that SDS monomers must cluster at the Novispirin surface. When a cluster of sufficient density has formed, it presumably generates enough anionic surface area to contact other Novispirin molecules (see below). For LTAC, the cooperative transition overlaps with the cmc under all conditions tested, suggesting that monomers may cluster to a small extent on Novispirin but are superseded by micelles above the cmc. This confirms that a supramolecular structure is required to overcome the electrostatic repulsions between positive side chains and the cationic headgroup of LTAC. The cooperative nature of Novispirin structure formation as a function of lipid

Table 6: Diffusion of Novispirin (c = 2.5 mM) in LTAC, pH 5.7

c_{LTAC}[a] (mM)	η[b] (mPa s)	$D_{obs,novi}$[c] (10^{-10} m^2 s^{-1})	$D_{obs,LTAC}$[d] (10^{-10} m^2 s^{-1})	R_h[e] Novispirin (nm)	R_h LTAC[f] micelles (nm)
0	1.13	1.75		1.10	
18	1.15	1.84	3.20	1.03	
97	1.26	1.65	1.39	1.05	1.46
174	1.37	1.47	1.13	1.08	1.54
247	1.50	1.32	0.99	1.10	1.56
322	1.63	1.33	0.89	1.00	1.57
395	1.78	1.19	0.80	1.04	1.57
478	1.96	1.09	0.74	1.03	1.53
575	2.18	0.94	0.66	1.07	1.53
639	2.34	0.87	0.60	1.07	1.56
711	2.53	0.71	0.55	1.22	1.59
798	2.78	0.60	0.44	1.31	1.80
880	3.02	0.55	0.41	1.31	1.75
1000	3.40	0.46	0.37	1.40	1.74

[a] Concentration of LTAC in millimoles per liter. [b] Viscosity of LTAC solution as calculated from eq 3. [c] Observed Novispirin diffusion constant. [d] Observed LTAC diffusion constant. [e] Hydrodynamic radius of Novispirin calculated from the Stokes−Einstein equation. [f] Hydrodynamic radius of LTAC micelles calculated from the Stokes−Einstein equation separating the contribution of the monomeric LTAC and the micellar LTAC by eq 4.

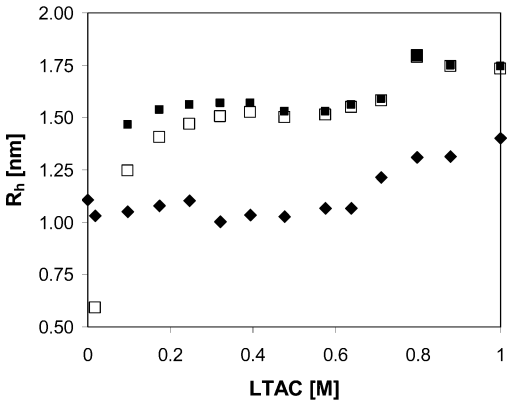

FIGURE 9: Hydrodynamic radii of Novispirin (filled diamonds) and LTAC micelles (filled squares) calculated from the diffusion constants by applying the Stokes−Einstein equation versus the concentration of LTAC. Open squares indicate the apparent hydrodynamic radius for LTAC, which is a population-weighted average of monomeric and micellar form.

concentration is less straightforward to explain, since the amount of peptide is not limiting for Novispirin oligomer formation at the vesicle surface at low-lipid concentrations. We can only speculate that extensive coating of the vesicle surface with Novispirin at very low-lipid concentrations can actually block structural transitions for steric reasons.

The Aggregated State: An Alternative to the Random-Coil and α-Helix. Pure DOPG leads to the formation of water-insoluble, β-sheet-rich aggregates with Novispirin. The same happens with SDS at certain protein/detergent ratios, although the Novispirin−SDS precipitate can be redissolved by adding more detergent. Variations in the amount of secondary structure in DOPG and SDS can be ascribed to differences in the concentrations of detergent versus lipid. LPS, however, which contains a small number of negative charges distributed in a matrix of neutral saccharides, is able to induce structure in its pure form at very low concentrations without forming precipitates to the same extent (although there may be a small amount of aggregation around 0.075 mM LPS, as the CD spectrum at this concentration does not cross the isodichroic point, unlike all other LPS concentrations). Thus, the ability to form aggregates is most likely promoted by electrostatically complementary "sandwich" structures between positively charged Novispirin and negatively charged lipids/detergents. For SDS, this is only possible at relatively low concentrations; at higher SDS concentrations, Novispirin becomes diluted out by SDS molecules, and SDS micelles form, which by themselves are solubilizing due to their high concentration of negative charge. Because of the high degree of light-scattering of DOPG vesicles, we were unable to determine whether higher concentrations of DOPG likewise lead to Novispirin solubilization and α-helix formation.

The aggregation phenomenon is unlikely to have biological significance, since uniformly anionic vesicles do not occur in nature. Nevertheless, it demonstrates that amphiphilic molecules not only necessarily just induce α-helical structure when bound to proteins but also allow them to access other conformational states, depending on the ratio between protein/peptide and amphiphile. SDS at submicellar concentrations has been shown to stimulate fibrillation of proteins (*59*, *60*), and anionic lipid vesicles stimulate the fibrillation of globular proteins and peptides, which at sufficiently high concentrations can even take up and incorporate the lipid in the fibril structures (*61*, *62*).

Novispirin Shows a Versatile Ability To Form Helical Structure in Detergents. Novispirin is able to form regular secondary structures in both anionic, zwitterionic, nonionic, and cationic detergents and phospholipids. The formation of secondary structure proceeds readily if the amphiphilic compounds are negatively charged. Both anionic detergents as SDS and anionic lipids as DOPG can induce secondary structure formation at relatively low concentrations; the latter however only if "diluted" by the zwitterionic DOPC.

The affinity of Novispirin toward negatively charged surfaces is not surprising, since Novispirin at pH 7.5 carries eight positive charges opposed by only one negative charge. Interestingly, Novispirin needs at least 20−40% anionic lipids to form secondary structure, which covers the fraction (around 25%) of anionic lipids present in *E. coli* inner membranes. Our lipid compositions deviate from bacterial membranes in that we used phosphatidylcholine rather than phosphatidylethanolamine due to phosphatidylcholine's superior bilayer-forming properties and the inability to extrude vesicles with high fractions of phosphatidylethanolamine. However, 10−20% of the latter lipid does not affect Novispirin structure.

The pure zwitterionic lipid (DOPC) is not able to induce structure in Novispirin. Uncharged (DM) and zwitterionic (DPS) detergents, however, do induce secondary structure in Novispirin. More counterintuitively, the cationic detergents LTAC and LTAB can likewise induce the formation of secondary structure. The LTAC/LTAB concentration needed to induce structure is strongly pH-dependent. At pH 7.5, a far lower amount of detergent is sufficient than at pH 5.7 (Figure 4). This indicates that the histidine side chain plays an important role in this interaction, since it is the only group titrating in this pH area. In 270 mM LTAC, the chemical shift of the two imidazole protons ($H^{\delta 2}$ and $H^{\epsilon 1}$) titrate with pH to give an apparent pK_a of 6.37 (data not shown). The chemical shift changes are likely to arise from a combination of protonation−deprotonation, association−dissociation, and

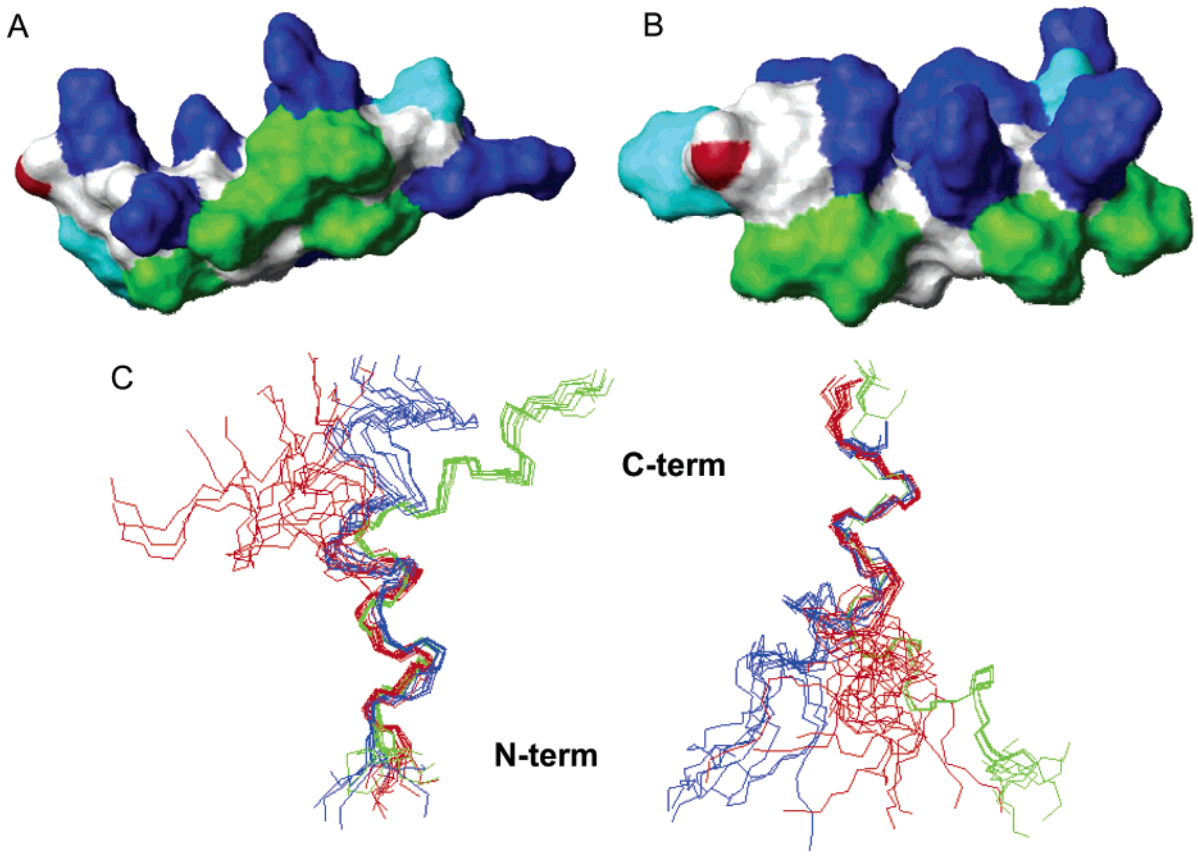

FIGURE 10: Novispirin in SDS (A) and LTAB (B). Contact surface. Green surface regions correspond to Ile and Leu residues, cyan corresponds to Asn and Tyr, red denotes the negatively charged C-terminus, and blue denotes positively charged side chains. The amphipatic nature of the Novispirin helix is evident. The spatial distribution of the positively charged side chains is much narrower in LTAB than in SDS. (C) A superposition of Novispirin in SDS (red), LTAB (blue), and TFE (green). For each structure, a bundle of the 10 best structures is shown. In the left panel, the N-terminal residues are superimposed; in the right panel, the C-terminal residues are superimposed.

folding−unfolding equilibria. However, the protonation−deprotonation generally give rise to the largest shift changes, making the value of 6.37 a reasonable estimate of the imidazole ring's pK_a. Since no positively charged biological membranes are known, the biological significance of this behavior is unknown. However, the observations reveal a surprisingly broad susceptibility of small peptides to form helical structures in micellar environments.

Structure Comparison. CD spectra of Novispirin in SDS, LTAC, and TFE revealed subtle differences. Access to atomic-level structures could elucidate the basis for these differences. Since only the structure in TFE is available (*30*), we have determined the high-resolution NMR structures of Novispirin in two different micellar solutions: SDS and LTAB. In both cases, there are well-defined helical regions interrupted by a less well-defined region around residues 10−12, in agreement with the TFE structure. While the kink in the helix is very well-defined for Novispirin in TFE, it is less so in SDS. This might reflect actual mobility, since the spectra were recorded at 50 °C. Also, recently published molecular dynamics simulations (*63*) point at a higher flexibility of Novispirin G-10 in SDS micelles. It has been pointed out that in the structure of Novispirin in TFE, I13 fills a void in the hydrophobic face of the molecule caused by the I10G mutation (*30*). Such an interaction might be the reason for the observed rigidity of the Novispirin structure. In micellar environments, however, the hydrophobic chains of the detergent molecules can take over this role, thus allowing a more flexible structure of the peptide itself. The structure in LTAB is better-defined. A reason for this might be that only certain orientations of the peptide backbone allow sufficient separation of the positive charges on the peptide from each other and from the positively charged micellar surface; thus, conformational freedom is severely restricted. As noted above, the introduction of an additional positive charge in the middle of the sequence by protonating H12 (at lower pH) greatly reduces the formation of structure at a given LTAC concentration. Figure 10A,B shows the structures of Novispirin in SDS and LTAB. Besides illustrating the amphipathic nature of the helix, it also shows a much narrower spatial distribution of the positively charged side chains when in contact with LTAB.

Figure 10C shows an overlay of the structures of Novispirin in SDS, LTAB, and TFE. It is evident that the structure is better-defined in TFE than in LTAB and SDS. The sequence plots (Figure 6 in this paper and Figure 2B in ref *30*) suggest that Novispirin in LTAB consists of two distinct helical regions of approximately the same number of amino acids, whereas Novispirin in both SDS and TFE consists of a well-defined N-terminal helix and a much less well-defined and smaller (in terms of its number of amino acids) C-terminal helix. The angle between the two helical fragments is different in all three cases, which might be a consequence of the special role of I13 (see above). Thus, although the general structure of the peptide is very similar under all three conditions, there are changes from one structure to another, which reflect the subtle changes observed in the far-UV CD spectra.

Novispirin Is Embedded in the SDS Micelle. It becomes clear that the key to understanding Novispirin's behavior lies in its interaction with the detergent micelles. Three types of experiments were performed to learn more about the relative orientation of Novispirin and the micelle: the backbone H^N exchange was determined qualitatively from TOCSY spectra, paramagnetic Mn^{2+} ions were added to the solution, and NOEs between SDS and Novispirin were investigated.

The H^N exchange data (Figure 8) revealed that not a single backbone H^N showed exchange with the bulk solvent. In a control experiment under identical conditions but without SDS, strong exchange peaks could be seen. Protection from exchange can signify a very stable hydrogen bond brought about by regular secondary structure or isolation from the bulk solvent. The two short helical stretches observed here are, however, unlikely to provide enough structural stability to explain the absence of H^N exchange by the existence of very stable hydrogen bonds. It is more likely that the backbone H^N atoms are situated inside the micelle, away from the bulk solvent. Only labile side-chain protons from arginine could be found to exchange with the solvent. This is indeed expected, since the positive charges in the vicinity of these atoms are supposed to be situated at the surface of the SDS micelle, where they can interact with the anionic sulfate headgroup. No lysine H^{ζ} could be observed in any of the spectra.

Additional evidence for a micelle-embedded conformation comes from NOESY spectra with nondeuterated SDS. As summarized in Table 5, cross-peaks could be detected from Novispirin hydrogen atoms to SDS hydrogen atoms. No NOEs could be detected from backbone H^N atoms to SDS atoms. However, nearly all visible side-chain atoms of Novispirin with a chemical shift bigger than 5 ppm (R5,6,8 H^{ϵ}, H12 $H^{\delta 2}$, $H^{\epsilon 1}$, Y17 $H^{\delta 1,2}$, $H^{\epsilon 1,2}$) showed cross-peaks to SDS. Cross-peaks to the aliphatic side chains could not be detected due to severe spectral distortion by the strong SDS signals. Therefore, neither the absence nor presence of such NOEs can be confirmed. Most NOEs show to the overlapping CH_2-group signals from CH_2-4−11 of SDS. Only weak interactions with 2-CH_2 and 3-CH_2 groups could be established. This could be due to the fact that the first group of signals yields a stronger cross-peak owing to the high amount of hydrogen atoms contributing to this peak, while signals observed from only one group are not strong enough. In a mobile ensemble, cross-peaks to several different atoms can be expected that do not necessarily point at short distances that have to be fulfilled simultaneously. No cross-peaks could be seen to SDS−CH_3 group. This could point at the fact that Novispirin does not protrude that deeply into the micelle but could also just mean that signals are too weak to be detected.

The visible cross-peaks, however, present strong evidence for a micelle-embedded structure. Under the high-salt concentration used for the NMR experiments, the cmc of SDS (around 0.1 mM) is too low to allow monomeric SDS to cause these cross-peaks.

The addition of paramagnetic Mn^{2+} ions gave another indication as to where in the micelle Novispirin is situated. Mn^{2+} was titrated into the solution until a relative difference in the ratio of remaining-to-original signal intensity could be seen between different peptide atoms. In the case of SDS, this proved to be at 0.5 mM. Probably, the Mn^{2+} ions stick to the surface of the SDS micelle and thus form a much higher local concentration. The data recorded in the presence of Mn^{2+} ions point toward a micelle-embedded structure, with the first helical stretch being buried in the micelle, a surface-exposed hinge around G10 and I11, and thereafter the second helical stretch being oriented in parallel to the surface, showing alternating protection and lack of it. The C-terminal residues are not protected at the backbone level; the presence of a negative charge at the C-terminus would also suggest that the C-terminus points away from the anionic micellar surface. The apparent low protection might also be caused by Mn^{2+} ions interacting with the C-terminus. In either case, the backbone of the C-terminus is exposed to the bulk solution. However, the aromatic side-chain atoms of Y17 are only moderately influenced by the presence of Mn^{2+}, which points at an interaction of the phenyl ring with the micelle. This interaction is also corroborated by NOEs from the aromatic protons of Y17 to SDS protons.

Finally, the diffusion constants obtained on Novispirin in SDS and the SDS micelle in the same sample are equal, which is strongly supporting a firm attachment of Novispirin to the SDS micelle.

In summary, the data point at a conformation where amino acids 2−8 (roughly speaking, the first helix) are buried in the micelle, whereas amino acids 9−18 (the kink and the second helix) are situated on the surface of the micelle.

Novispirin Is Only Loosely Associated with the LTAC Micelle. Similar experiments as those for Novispirin in SDS were also conducted to investigate Novispirin in LTAC micelles. The results, however, pointed in a very different direction.

The H^N exchange was likewise estimated qualitatively from TOCSY spectra. Unlike SDS, several backbone H^N were found to exchange with bulk water in the presence of LTAC micelles. The spectrum shown in Figure 8G,H exhibits a range of exchange peaks. The only backbone H^N atoms, which definitely do not exchange, are from the three hydrophobic residues I6, I11, and I13 and from the three C-terminal residues K16, Y17, and G18. The labile side-chain protons of arginine again showed exchange with the solvent.

In LTAB, 8 times more Mn^{2+} was needed than in SDS to elicit an effect on the peak signals, probably due to repulsion between the cationic LTAC headgroup and Mn^{2+}. Only very few residues were protected against Mn^{2+}, namely, I6, I13, and I14.

A NOESY spectrum of Novispirin in nondeuterated LTAC did not show any cross-peaks from Novispirin to LTAC. As for SDS, neither the presence nor the absence of NOEs from LTAC to aliphatic side-chain atoms could be unambiguously proven due to signal overlap and severe spectral distortions brought about by the high concentration of the detergent.

From the results of the three experiments (exchange, addition of Mn^{2+}, and NOESY), it is doubtful whether Novispirin actually is bound to the LTAC micelle at all. Therefore, diffusion measurements were conducted to investigate whether Novispirin is bound to the LTAC micelle or whether it is free in solution. A number of pulsed-field gradient NMR measurements were conducted to determine the diffusion coefficient of Novispirin in the presence of increasing concentrations of LTAC. At pH 5.7, it was found that the apparent hydrodynamic radius of Novispirin remains

constant up to approximately 600 mM LTAC; hereafter, it increases. This points toward the formation of larger aggregates, most probably peptide−micelle clusters. This is further corroborated by the fact that also apparent micellar hydrodynamic radii increase at this point. However, Novispirin still diffuses faster than the micelle and is thus not tightly bound; otherwise, Novispirin's and the micelle's diffusion coefficients and apparent hydrodynamic radii should be equal. Comparing with the 1D NMR spectra at different LTAC concentrations (Figure 4), it can be seen that a dispersion of NMR signals begins already at lower levels of LTAC. We suggest that there is an equilibrium between a micelle-associated, folded and a free, unfolded form, that gradually is shifted toward the micelle-associated, folded form upon increasing detergent concentrations. This is in agreement with far-UV CD titration experiments in up to 1 M LTAC at pH 5.7 which show that the degree of α-helicity increases in an essentially linear fashion between 0 and 1 M LTAC and has not yet reached a plateau level at 1 M LTAC (Figure 3C).

Combining these pieces of information, it seems likely that Novispirin is weakly associated with the micelle in equilibrium between bound and free form. However, even such a weak association appears sufficient to induce an overall folded structure. The induction of structure is not an artifact of the high concentration of detergent used (e.g., through reduction of water activity or binding of the counterion bromide), since it is also observed at 20−40 mM LTAC at pH 7.5 under CD conditions, that is, much lower peptide concentrations; furthermore, halide ions at molar concentrations do not by themselves induce helical structure in Novispirin (data not shown). The strong increase in binding affinity upon increasing the pH from 5.7 to 7.5, which is accompanied only by the deprotonation of the single histidine residue, also points to very specific interactions between LTAC and Novispirin. The somewhat counterintuitive interactions with a positively charged detergent are of great principal interest. The fact that such interactions can be observed might lead to a reevaluation of the driving forces behind peptide/membrane association. Understanding these driving forces will in turn be rewarded with the ability to design target-specific antimicrobial peptides.

ACKNOWLEDGMENT

We thank Dr. Peter Güntert for help with the energy-minimization of the final structures and Dr. Yiannis Kaznessis for providing his results prior to publication. We thank Professor Norbert Müller for valuable discussions and Henning Sørensen and Tina Johnson for initial experiments with Novispirin in LTAB.

REFERENCES

1. Mygind, P. H., Fischer, R. L., Schnorr, K. M., Hansen, M. T., Sönksen, C. P., Ludvigsen, S., Raventós, D., Buskov, S., Christensen, B., De Maria, L., Taboureau, O., Yaver, D., Elvig-Jørgensen, S. G., Sørensen, M. V., Christensen, B. E., Kjærulff, S., Frimodt-Møller, N., Lehrer, R. I., Zasloff, M., and Kristensen, H.-H. (2005) Plectasin is a peptide antibiotic with therapeutic potential from a saprophytic fungus, *Nature 437*, 975−980.
2. Zasloff, M. (2002) Antimicrobial peptides of multicellular organisms, *Nature 415*, 389−395.
3. Bals, R. (2000) Epithelial antimicrobial peptides in host defense against infection, *Respir. Res. 1*, 141−150.
4. Volles, M. J., and Lansbury, P. T. (2002) Vesicle permeabilization by protofibrillar α-synuclein is sensitive to Parkinson's disease-linked mutations and occurs by a pore-like mechanism, *Biochemistry 41*, 4595−4602.
5. Volles, M. J., and Lansbury, P. T. (2003) Zeroing in on the pathogenic form of α-synuclein and its mechanism of neurotoxicity in Parkinson's disease, *Biochemistry 42*, 7871−7878.
6. Shai, Y. (1999) Mechanism of the binding, insertion and destabilization of phospholipid bilayer membranes by α-helical antimicrobial and cell non-selective membrane-lytic peptides, *Biochim. Biophys. Acta 1462*, 55−70.
7. Matsuzaki, K. (1999) Why and how are peptide-lipid interactions utilized for self-defense? Magainins and tachyplesins as archetypes, *Biochim. Biophys. Acta 1462*, 1−10.
8. Huang, H. W. (2000) Action of antimicrobial peptides: Two-state model, *Biochemistry 39*, 8347−8352.
9. Shai, Y. (2002) Mode of action of membrane active antimicrobial peptides, *Biopolymers 66*, 236−248.
10. Yang, D., Chertov, O., and Oppenheim, J. J. (2001) The role of mammalian antimicrobial peptides and proteins in awakening of innate host defenses and adaptive immunity, *Cell. Mol. Life Sci. 58*, 978−98.
11. Jerala, R., and Porro, M. (2004) Endotoxin neutralizing peptides, *Curr. Top. Med. Chem. 4*, 1173−1184.
12. Chertov, O., Yang, D., Howard, O. M., and Oppenheim, J. J. (2000) Leukocyte granule proteins mobilize innate host defenses and adaptive immune responses, *Immunol. Rev. 177*, 68−78.
13. Park, I. Y., Cho, J. H., Kim, K. S., Kim, Y.-B., Kim, M. S., and Kim, S. C. (2004) Helix stability confers salt resistance upon helical antimicrobial peptides, *J. Biol. Chem. 279*, 13896−13901.
14. Wu, M., Maier, E., Benz, R., and Hancock, R. E. W. (1999) Mechanism of interaction of different classes of cationic antimicrobial peptides with planar bilayers and with the cytoplasmic membrane of *Escherichia coli*, *Biochemistry 38*, 7235−7242.
15. Lee, I. H., Cho, Y., and Lehrer, R. I. (1997) Effects of pH and salinity on the antimicrobial properties of clavanins, *Infect. Immun. 65*, 2898−2903.
16. Lee, M.-T., Chen, F.-Y., and Huang, H. W. (2004) Energetics of pore formation induced by membrane active peptides, *Biochemistry 43*, 3590−3599.
17. Henzler-Wildman, K. A., Martinez, G. V., Brown, M. F., and Ramamoorthy, A. (2004) Perturbation of the hydrophobic core of lipid bilayers by the human antimicrobial peptide LL-37, *Biochemistry 43*, 8459−8469.
18. Heller, W. T., He, K., Ludtke, S. J., Harround, T. A., and Huang, H. W. (1997) Effect of changing the size of lipid headgroup on peptide insertion into membranes, *Biophys. J. 73*, 239−244.
19. Buffy, J. J., Waring, A. J., Lehrer, R. I., and Hong, M. (2003) Immobilization and aggregation of the antimicrobial peptide protegrin-1 in lipid bilayers investigated by solid-state NMR, *Biochemistry 42*, 13725−13734.
20. Hancock, R. E. W., and Rozek, A. (2002) Role of membranes in the activities of antimicrobial cationic peptides, *FEMS Microbiol. Lett. 206*, 143−149.
21. Jing, W., Hunter, H. N., Hagel, J., and Vogel, H. J. (2003) The structure of the antimicrobial peptide Ac-RRWWRF-NH_2 bound to micelles and its interactions with phospholipid bilayers, *J. Pept. Res. 61*, 219−229.
22. Watson, R. M., Woody, R. W., Lewis, R. V., Bohle, D. S., Andreotti, A. H., Ray, B., and Miller, K. W. (2001) Conformational changes in pediocin AcH upon vesicle binding and approximation of the membrane-bound structure in detergent micelles, *Biochemistry 40*, 14037−14046.
23. Montserret, R., McLeish, M. J., Böckmann, A., Geourjon, C., and Penin, F. (2000) Involvement of electrostatic interactions in the mechanism of peptide folding induced by sodium dodecyl sulfate binding, *Biochemistry 39*, 8362−8374.
24. Lewis, R. N., Kiricsi, M., Prenner, E. J., Hodges, R. S., and McElhaney, R. N. (2003) Fourier transform infrared spectroscopic study of the interactions of a strongly antimicrobial but weakly hemolytic analogue of gramicidin S with lipid micelles and lipid bilayer membranes, *Biochemistry 42*, 440−449.
25. Zhong, L., and Johnson, W. C. (1992) Environment affects amino acid preference for secondary structure, *Proc. Natl. Acad. Sci. U.S.A. 89*, 4462−4465.
26. Yonath, A., Podjarny, A., Honig, B., Sielecki, A., and Traub, W. (1977) Crystallographic studies of protein denaturation and renaturation. 2. Sodium dodecyl sulfate induced structural changes in triclinic lysozyme, *Biochemistry 16*, 1418−1424.

27. Pervushin, K. V., Orekhov, V. Y., Popov, A. I., Musina, L. Y., and Arseniev, A. S. (1994) Three-dimensional structure of (1-71)bacterioopsin solubilized in methanol/chloroform and SDS micelles determined by ^{15}N-^{1}H heteronuclear NMR spectroscopy, *Eur. J. Biochem. 219*, 571−583.
28. Keifer, P., Peterkovsky, A., and Wang, G. (2004) Effects of detergent alkyl chain length and chemical structure on the properties of a micelle-bound bacterial membrane targeting peptide, *Anal. Biochem. 331*, 33−39.
29. Travis, S. M., Anderson, N. N., Forsyth, W. R., Espiritu, C., Conway, D., Greenberg, E. P., McCray, P. B. J., Lehrer, R. I., Welsh, M. J., and Tack, B. F. (2000) Bacteriocidal activity of mammalian cathelicidin-derived peptides, *Infect. Immunol. 68*, 2748−2755.
30. Sawai, M. V., Waring, A. J., Kearney, W. R., McCray, P. B. J., Forsyth, W. R., Lehrer, R. I., and Tack, B. F. (2002) Impact of single-residue mutations on the structure and function of ovispirin/novispirin antimicrobial peptides, *Protein Eng. 15*, 225−232.
31. Jasanoff, A., and Fersht, A. R. (1994) Quantitative determination of helical propensities from trifluoroethanol titration curves, *Biochemistry 33*, 2129−2135.
32. Hirota, N., Mizuno, K., and Goto, Y. (1998) Group additive contributions to the alcohol-induced α-helix formation of melittin: Implication for the mechanism of the alcohol effects on proteins, *J. Mol. Biol. 275*, 365−378.
33. Gavin, P., and Better, M. (2000) Production of antifungal recombinant peptides in *Escherichia coli*, *J. Biotechnol. 79*, 127−136.
34. Jauregui-Adell, J., and Marti, J. (1975) Acidic cleavage of the aspartyl-proline band and the limitations of the reaction, *Anal. Biochem. 69*, 468−473.
35. Sambrook, J., Fritsch, E. F., and Maniatis, T. (1989) *Molecular Cloning*, Cold Spring Harbor Laboratory Press, New York.
36. Svendsen, I., and Breddam, K. (1992) Isolation and amino acid sequence of a glutamic acid specific endopeptidase from *Bacillus licheniformis*, *Eur. J. Biochem. 204*, 165−171.
37. Byler, D. M., and Sussi, H. (1986) Examination of the secondary structure of proteins by deconvolved FTIR spectra, *Biopolymers 25*, 469−487.
38. Hwang, T. L., and Shaka, A. J. (1995) Water suppression that works. Excitation sculpting using arbitrary wave-forms and pulsed-field gradients, *J. Magn. Reson. 112*, 275−279.
39. Emsley, L., and Bodenhausen, G. (1992) Optimisation of shaped selective pulses for NMR using a quaternion description of their overall propagators, *J. Magn. Reson. 97*, 135−148.
40. Piotto, M., Saudek, V., and Sklenar, V. (1992) Gradient-tailored excitation for single-quantum NMR spectroscopy of aqueous solutions, *J. Biomol. NMR 2*, 661−666.
41. Griesinger, C., Otting, G., and Wüthrich, K. (1988) Clean TOCSY for 1H spin system identification in macromolecules, *J. Am. Chem. Soc. 110*, 7870−7872.
42. Wüthrich, K. (1986) *NMR of Proteins and Nucleic Acids*, Wiley, New York.
43. Bartels, C., Xia, T.-H., Billeter, M., Günter, P., and Wüthrich, K. (1995) The program XEASY for computer-supported NMR spectral of biological macromolecules, *J. Biomol. NMR 5*, 1−10.
44. Jerschow, A., and Müller, N. (1997) Suppression of convection artifacts in stiumlated-echo diffusion experiments: Double-stimulated-echo experiments, *J. Magn. Reson. 125*, 372−375.
45. Fersht, A. R. (1999) *Structure and Mechanism in Protein Science. A Guide to Enzyme Catalysis and Protein Folding*, Freeman & Co., New York.
46. Keller, R. (2004) *The Computer Aided Resonance Assignment Tutorial*, Cantina Verlag, Goldau.
47. Cornilescu, G., Delagio, F., and Bax, A. (1999) Protein backbone angle restraints from searching a database for chemical shift and sequence homology, *J. Biomol. NMR 13*, 289−302.
48. Güntert, P., Braun, P., and Wüthrich, K. (1991) Efficient computation of three-dimensional protein structures in solution from nuclear magnetic resonance data using the program DIANA and the supporting programs CALIBA, HABAS and GLOMSA, *J. Mol. Biol. 217*, 517−530.
49. Güntert, P., Billeter, M., Ohlenschläger, O., Brown, L. R., and Wüthrich, K. (1998) Conformational analysis of proteins and nucleic acid fragments with the new grid search algorithm FOUND, *J. Biomol. NMR 12*, 543−548.
50. Güntert, P., Mumenthaler, C., and Wüthrich, K. (1997) Torsion angle dynamics for NMR structure calculation with the new program DYANA, *J. Mol. Biol. 273*, 283−298.
51. Cornell, W. D., Cieplak, P., Bayly, C. I., Gould, I. R., Merz, K. M., Ferguson, D. M., Spellmeyer, D. C., Fox, T., Caldwell, J. W., and Kollman, P. A. (1995) A second generation force field for the simulation of proteins, nucleic acids, and organic molecules, *J. Am. Chem. Soc. 117*, 5179−5197.
52. Luginbühl, P., Güntert, P., Billeter, M., and Wüthrich, K. (1996) The new program OPAL for molecular dynamics simulations and energy refinements of biological macromolecules, *J. Biomol. NMR 8*, 136−146.
53. Laskowski, R. A., MacArthur, M. W., Moss, D. S., and Thornton, J. M. (1993) PROCHECK: A program to check the stereochemical quality of protein structures, *J. Appl. Crystallogr. 26*, 283−291.
54. Provencher, S. W., and Glöckner, J. (1981) Estimation of globular protein secondary structure from circular dichroism, *Biochemistry 20*, 33−37.
55. Santos, N. C., Silva, A. C., Castanho, M. A., Martins-Silva, J., and Saldanha, C. (2003) Evaluation of lipopolysaccharide aggregation by light scattering spectroscopy, *ChemBioChem 4*, 96−100.
56. Lindberg, M., Biverståhl, H., Gräslund, A., and Mäler, L. (2003) Structure and positioning comparison of two variants of penetratin in two different membrane mimicking systems by NMR, *Eur. J. Biochem. 270*, 3055−3063.
57. Rosen, M. J. (1988) *Surfactants and Interfacial Phenomena*, Wiley, New York.
58. Tanford, C. (1970) Protein denaturation. Part C. Theoretical models for the mechanism of denaturation, *Adv. Protein Chem. 24*, 1−95.
59. Pertinhez, T. A., Bouchard, M., Smith, R. A. G., Dobson, C. M., and Smith, L. J. (2002) Stimulation and inhibition of fibril formation by a peptide in the presence of different concentrations of SDS, *FEBS Lett. 529*, 193−197.
60. Yamamoto, S., Kasegawa, K., Yamaguchi, I., Tsutsumi, S., Kardos, J., Goto, Y., Gejyo, F., and Naiki, H. (2004) Low concentrations of sodium dodecyl sulfate induces the extension of β_2-microglobulin-related amyloid fibrils at neutral pH, *Biochemistry 43*, 11075−11082.
61. Zhao, H., Tuominen, E. K. J., and Kinnunen, P. K. J. (2004) Formation of amyloid fibers triggered by phosphatidylserine-containing membranes, *Biochemistry 43*, 10302−10307.
62. Sparr, E., Engel, M. F. M., Sakharov, D. V., Sprong, M., Jacobs, J., de Kruijff, B., Höppner, J. W. M., and Killian, J. A. (2004) Islet amyloid polypeptide-induced membrane leakage involves uptake of lipids by forming amyloid fibers, *FEBS Lett. 577*, 117−120.
63. Khandelia, H., and Kaznessis, Y. N. (2005) Molecular dynamics simulations of helical antimicrobial peptides in SDS micelles: What do point mutations achieve? *Peptides 26*, 2037−2049.
64. Koradi, R., Billeter, M., and Wüthrich, K. (1996) MOLMOL: A program for display and analysis of macromolecular structures, *J. Mol. Graphics 14*, 51−55.

BI051876R